Linköping university
Department of Management and Engineering
Master's Thesis, 30 ECTS | Solid Mechanics
Spring 2024 | LIU-IEI-TEK-A–24/04997–SE
SE-581 83 Linköping, +46 13 28 10 00, www.liu.se

PROCESS SIMULATION OF ADDITIVE MANUFACTURING FOR POLYMERS

By

SUMANT BALLI

Examiner:	Robert Eriksson
Academic Supervisor:	Daniel Leidermark
Industrial Supervisor:	Mohammad Rouhi

Date Published: 9th October 2024

Linköpings universitet
581 83 Linköping
Sweden

ABSTRACT

Additive Manufacturing (AM), also known as 3D printing, has transformed traditional manufacturing by enabling the fabrication of intricate and customized parts with unprecedented design freedom. However, comprehending the underlying additive manufacturing processes, including thermal behavior, material interactions, and residual stresses, is quite challenging due to their inherent complexity. This thesis work focuses on using finite element (FE) simulations with Abaqus to enhance AM processes involving polymers. The aim is to develop accurate FE modeling and process simulation to predict and optimize thermal and mechanical phenomena during AM, which directly impacts product quality and waste generation.

A detailed FE model for Nylon PA6 has been developed, incorporating its temperature-dependent thermal and mechanical properties. A sequentially coupled thermo-mechanical approach has been utilized to simulate the heat transfer, thermal distortion, and residual stress accumulation process in AM. The simulated results are compared with experimental results to analyze temperature distribution and its correlation with mechanical deformation. Realistic boundary conditions, such as preheating the build plate and controlled thermal environments, have been incorporated into the simulations to enhance accuracy.

The simulation accurately predicted the thermal and mechanical analyses, aligning with the experimental trend data and mechanical deformation. However, there were notable discrepancies in more complex thermal interactions. By refining boundary conditions, introducing flexible constraints, and adjusting coefficients of thermal expansion (CTE), the model was able to more accurately capture the real distortion patterns observed in printed parts. This underscores the effectiveness of FE simulations as a tool to enhance the accuracy and reliability of AM processes. Additionally, these simulations provide valuable insights into optimal conditions for manufacturing, cost-cutting, and improvements in the quality and uniformity of the final product.

This research contributes to a better understanding of the optimization of AM processes and provides important tools for both academic research and industry applications. It promotes the direct adoption of AM technologies and fosters more efficient and sustainable manufacturing practices.

ACKNOWLEDGEMENTS

I would like to take this opportunity and thank my examiner at Linköping University, Robert Eriksson. His contribution was invaluable, and the patience he offered with both non-technical and technical issues, as well as the scrupulous treatment of paperwork, helped me manage to finish on time. Robert's dedication and support were instrumental in helping navigate me through the administrative matters encountered during my thesis, and this contributed to its successful completion.

I would like to give my deepest gratitude to my academic supervisor at Linköping University, Daniel Leidermark. His knowledge of mechanical engineering, and continuing to serve as a reliable sounding board throughout my research, provided invaluable insights and guidance. The support from Daniel and his reflective feedback has been of paramount importance concerning the direction of my project and overcoming the challenges during my research.

I would also like to express my heartfelt appreciation to my supervisor from RI.SE, Mohammad Rouhi (Senior Researcher). His patience, mentorship, and technical guidance were crucial in the development and execution of this thesis. It was Mohammad's expert advice and encouragement that proved pivotal for steering this project to its successful outcome. Further, I also would like to acknowledge that this project is a part of the national SuRF-LSAM initiative funded by Vinnova/Produktion2030. The support and facilities provided by RI.SE were essential and crucial for carrying out this study.

I would also like to extend my appreciative words to the entire team at RI.SE for their excellent team spirit and an outstanding environment that is conducive to research. The inspiring and supportive atmosphere at RI.SE greatly benefited my work a lot and contributed to the overall success of my project.

Lastly, I want to express my special gratitude to my parents and friends. Their belief and support have always acted as a cornerstone for me. Right from my early university days, encouragement and enthusiasm to achieve my targets acted as a guiding force for me. Their continuous presence and positive influence have been crucial for my success, and their inspiration was very priceless for me at different junctures of my journey.

NOMENCLATURE

- FE - Finite element
- LSAM - Large scale additive manufacturing
- SuRF - Sustainable Resilient circular economy micro-factories
- AM - Additive manufacturing
- FDM - Fused deposition modeling
- PEI - Polyetherimide
- U - Specific internal energy
- q - heat flux density vector
- q_{gen} - Rate of heat production density
- k - Thermal conductivity
- T - Temperature
- ρ - Density
- $K_{pp}(\sigma)$ - Material's specific heat capacity
- $\dot{T}$ - Nodal vector of temperature
- D_c - Construction chamber
- $S(t)$ - External surface of the body
- K_b - Stefan-Boltzmann
- ϵ - Emissivity
- ϵ - Total strain in mechanical analysis
- λ - Plastic flow factor
- R - Thermal resistance
- h^* - Gap conductance coefficient
- d - clearance
- DOF - Degree of freedom
- CTE - Coefficient of thermal expansion
- E - Young's modulus
- ν - Poisson's ratio
- CNC - Computer numerical control

Contents

1 INTRODUCTION

This chapter provides an overview of the thesis work which includes the background of the company where the research is conducted, motivation, objective, and finally research question and approach undertaken for this research work.

1.1 About RI.SE

The Research Institutes of Sweden, also known as RISE, is an independent state-owned organization. RISE is one of 43 companies fully or partially owned by the Swedish government. It collaborates with academia, the commercial sector, and the government to support the development of technology, products, services, and processes that contribute to a competitive industry and a sustainable world. RISE plays a crucial role in assisting small and medium-sized businesses with their innovation processes.[1].

At present, RISE has around 3,300 employees across the country and in various foreign subsidiaries. These individuals include technicians, researchers, and other experts who are essential for developing future innovations. They apply scientific principles to help clients and partners overcome obstacles, implement a comprehensive strategy to solve complex problems and improve their competitive advantage.

1.2 Motivation

Additive Manufacturing, also known as 3D printing, has revolutionized traditional manufacturing processes by enabling the creation of complex and customized components, as well as providing unprecedented design flexibility. However, the inherently complex nature of the AM process poses challenges related to understanding thermal behavior, material interaction, and residual stress development.

To address these obstacles, Finite Element methods are used with accurate material models, emerging as a powerful tool. This critical approach enables the prediction and control of the outcome of AM processes to tackle these challenges. This project is a national part of SuRF-LSAM, which is already funded by Vinnova/Produktion2030.

The significance of this thesis lies in the fact that scaling the simulation results strategies with the AM process will have an immediate impact on manufacturing operations, allowing companies to efficiently improve their processes, reduce costs, and produce high-quality components.

Furthermore, by validating and comparing the results with experimental data, the aim is to ensure that the simulation outcomes align with real-world studies. This thesis project is expected to instill confidence in the developed framework, likely establishing it as a reliable tool, especially for researchers and engineers.

1.3 Objective

The main goal of this research is to investigate how using FE simulation and analysis in ABAQUS can improve AM processes for polymers. The focus is on enhancing product quality, reducing waste, and promoting efficient manufacturing practices. By achieving these objectives, both commercial enterprises and academic institutions can benefit from this technology.

- **Modeling:** Develop FE models that accurately capture the behavior of material (here Nylon PA6) used in the AM process. This includes factors such as thermal behavior, mechanical properties, and phase transformations.
- **Process Simulation:** Utilize Abaqus software to simulate the AM process by calculating heat transfer, thermal distortion, and residual stress. Implement a simulation approach that aligns with real-world AM techniques.
- **Validation:** Simulation results will be validated against the experimental data to ensure the accuracy and reliability of the simulation.

The findings, from this study will greatly enhance our understanding of additive manufacturing (AM) processes. This in turn will provide insights into optimizing manufacturing conditions and promoting the adoption of this revolutionary technology.

1.4 Research Question and Approach

The main aim of this study is to analyze the application of finite element FE simulation and analysis in Abaqus to improve the additive manufacturing process for polymers. The nature of the field of AM itself is very complex, especially concerning thermal aspects and distortion of materials and therefore, it is important to seek solutions to the problems at hand using better simulations. The following research questions are framed to proceed with our studies:

a. How does one improve FE simulation in Abaqus for the better prediction of thermal behavior and distortion in polymeric materials during their AM processes? The latter is in pursuit of answering the potential use of FE simulations in reflecting the complex thermal dynamics and resultant distortions during AM processes, to enhance the predictive accuracy of simulations which helps to improve the quality of the products.

b. How do alternative boundary conditions in FE simulations affect the accuracy of the distortion prediction in structure, and what is the best setup of these conditions reflecting real manufacturing scenarios? These conditions are normally simplified most of the time during simulations to remove the complexity of the model, leading to inaccuracies in the prediction of part distortions. The question goes to understand the conditions and best settings that offer closeness to real-life manufacture.

c. How might the integration of FE simulation and materials modeling in Abaqus contribute to waste reduction in polymer AM processes while maintaining or improving product quality? This question deals with the twofold objectives of minimal material waste coupled with better qualities of the product. Simulations allow research to come up with strategies that are both economically and ecologically viable.

d. How is the accuracy of FE simulations in Abaqus validated against experimental data for thermal analysis in polymer AM, and what are the challenges to this validation? To rely on the simulation prediction, we need to validate and compare it with the experimental data. This question shall discuss methodologies for the validation of thermal analysis predictions and obstacles that can/will be faced in such a process.

The approach is divided into the following ways:

- Developing accurate FE models that consider thermal behavior, mechanical properties, and phase transformations.
- The simulation of AM processes, concentrating on aspects such as temperature distribution in the thermal analysis and predicting distortion and residual stress in structural analysis.
- Validation against experimental data will ensure the reliability of the simulation framework, and optimization studies will be conducted to identify optimal process conditions.

1.5 Other Consideration

No ethical or gender-related issues are aroused by the work. Although it does not have a direct connection to such concerns, it contributes positively to the sustainable development of society by raising resource efficiency and reducing waste. It applies advanced techniques of simulation in optimizing the Large-Scale Additive Manufacturing process and hence tries to minimize the necessity of extended experiments by trial and error, which means less generation of waste materials. Numerical and computational aids for mechanical and thermal analysis are, therefore, utilized in the work to support the pursuit of more sustainable manufacturing processes and better utilization of polymer materials, by environmental sustainability goals.

2 THEORY

2.1 Background

The SuRF-LSAM project builds on the groundwork laid by OCEAN-LSAM, advancing the concept of circular economy micro-factories. While OCEAN-LSAM focused on developing the project framework and consortium, SuRF-LSAM takes it further by implementing the micro-factory concept through the establishment of recycling facilities in Sweden and Portugal. These facilities will demonstrate large-scale additive manufacturing of locally recycled ocean polymers across the value chain.

The objective of this project is to develop, test, and demonstrate a worldwide network of micro-factories that will implement a concept called Circular Economy. LSAM will be used to fabricate products out of recycled ocean and polymer waste. The proposal aims to establish two LSAM micro-factories in Sweden and Portugal for recycling local municipal waste into raw material for manufacturing in the same facility. This approach is intended to realize a demand-driven, circular production close to the local market, which reduces transportation times and avoids supply chain risks.

Challenges to be addressed in the project include the optimization of LSAM-qualified, recycled polyamide composites, improvement of printing quality, and establishment of a digital simulation model for enhanced material processing. Digital twin technology will be used to simulate how materials will behave during the LSAM process, minimizing the trial-and-error process.

The SuRF-LSAM project aims to establish a sustainable global network of micro-factories, contributing to Sweden's leadership in digitalization and a circular economy. It also aligns with several of the UN's sustainable development goals (SDGs), including SDG 9 (Industry, Innovation, and Infrastructure), SDG 11 (Sustainable Cities and Communities), SDG 12 (Responsible Consumption and Production), and SDG 14 (Life Below Water).

The SuRF-LSAM project was divided into five work packages (WP), each with specific goals [2]. WP1 managed the entire project to ensure efficient collaboration among all parties, timely delivery, and goal achievement. Under the leadership of RISE, WP2 focused on supply chain issues and sustainability, including cost, lead times, and environmental impact. It compared these factors using the Sustainability Parameters for Parts Analyses and Selection for Additive Manufacturing (SPARSAM) model against traditional methods. WP3, under the leadership of Ocean Tech Hub, worked on formulating and characterizing material compounding recipes for LSAM processes to reach optimal solutions for industrial use, as shown in Figure 1. WP4, led by RISE, focused on developing numerical and computational tools for mechanical and thermal analysis to optimize material and process design while reducing waste. It also aimed to develop a preliminary numerical simulation model of the LSAM and validate it to improve the process. WP5, led by Chalmers, focused on implementing a Circular micro-factory concept and involving

stakeholders to develop practical applications in Sweden and Portugal.

Figure 1: Developing recycled polyamide material

The AM process simulation is used to study the printing process and improve the process parameters and material characteristics before printing. The aim is to reduce the trial and error process during printing by learning from the process model and material behavior during simulation. Abaqus software is used for its fully embedded AM process simulation features, including fused deposition modeling (FDM) techniques for LSAM of polymers. The analysis technique used for modeling is the thermo-mechanical method. Thermo-mechanical simulations involve sequentially coupled thermal-stress analyses, consisting of transient heat transfer analysis followed by mechanical analysis in a static step using the temperature from the thermal stage as loads. Simulations can provide accurate geometrical features for the printing part and incorporate nonlinear temperature-dependent material properties for accurate material behavior.

2.2 Additive manufacturing

Additive manufacturing is the process of creating a three-dimensional solid object from the CAD file. This is achieved by building successive layers of material to form the desired object. Additive manufacturing offers several advantages over traditional manufacturing methods, including cost reduction, decreased production time, and fewer errors. However, the diversity of materials available for additive manufacturing is still limited, as some are still in the developmental stage.

Seven different additive manufacturing categories:

- Powder Bed Fusion
- Binder jetting
- Directed Energy Deposition
- Material Extrusion

- Sheet Lamination
- VAT Photopolymerization
- Material Jetting

This method differs from other traditional manufacturing strategies like injection, casting, and sintering because it involves adding material rather than subtracting it. Unlike these traditional methods, it doesn't require additional tooling separate from the machine used. Initially, it was mainly used for quick prototyping due to its cost-effectiveness for small batches and its quick product development process. However, it is now being used in various industries such as medical, automotive, aerospace, and customized applications due to technological advancements. Despite the increasing importance of additive manufacturing (AM), there are still questions about how to improve the quality of manufactured parts and reduce production cycle time.

Amidst these categories, the Material Extrusion method is being used in the current project. S.Scott Crump created the 3D printing method as FDM in the late 1980's [3]. The idea behind the FDM is to build three-dimensional structures by depositing thermoplastic materials one layer at a time as shown in Figure 2. The conventional technique of polymers and plastic extrusion served as the model for this approach. FDM is quite popular amongst other methods since it relatively and affordably creates functioning prototypes and complex geometries easily. FDM is used in many industries like aerospace, automotive industries, and health industries.

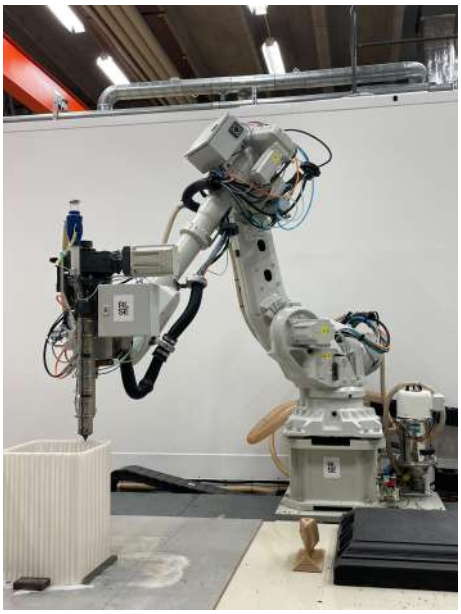

Figure 2: Robotic additive manufacturing process, demonstrating layer-by-layer deposition of polymer material at RISE

In FDM, a thermoplastic filament is melted and then successively extruded to form

a three-dimensional object as shown in Figure 2 and Figure 3. The design program exactly arranges the placement of the melted material, which solidifies quickly in a short time when it is deposited onto the layer printed previously. Through the progressive accumulation of material, this AM method makes it possible to create intricate forms and structures. Following the design criteria, the temperature-controlled nozzle precisely deposits the material by moving in the X, Y, and Z axes.

Figure 3: Printing of Eel Lounge chair in laboratory at RISE

2.3 Additive manufacturing simulation

The physical phenomena that occur during printing when activated by a robot need to be simulated accurately to predict their natural behaviors. It is crucial to consider the geometrical features involved in dissipating heat in the air and the convection between the environment and the part surface, as these thermal effects impact the process significantly. Additionally, the temperature-dependent rheological and mechanical properties of the material must be taken into consideration to reflect the real-world process. The speed of the robot, nozzle temperature, and layer height are among the most important process parameters that will affect the quality of the final part.

Factors such as air dissipation, heat transfer between surfaces, and thermal distortion of the part should also be considered. The simulation approach involves sequentially coupled thermo-mechanical analysis, which allows for an interaction between thermal and mechanical analyses. This approach enables a comprehensive analysis of FDM by integrating thermal, structural, and other physical aspects into the FE model. These considerations, as shown in the flowchart of Figure 4, provide a way for the simulation to predict process parameters, boundary conditions, and material behavior effects on the final part, which can help optimize the AM process.

The additive manufacturing (AM) process simulation involves numerous factors such as material characteristics, boundary conditions, component geometry complexity,

and deposition features, all of which have a significant impact on the features of the produced part. Conducting experiments to understand how each variable affects residual stress distribution and distortion inside the constructed medium is a time-consuming process. Therefore, FE analysis and other numerical analytic techniques serve as good substitutes for measuring and quantifying the impact of process factors. In recent decades, several methods and techniques have been developed to study the thermo-mechanical phenomena occurring during the AM process.

In FDM technology, the nozzle follows a predetermined printing path while the filament is heated to a semi-molten condition before being ejected. After deposition, heat energy dissipates through conduction within and between filaments, as well as through convection and radiation between the filament and the surrounding environment. The heating and cooling process causes high-temperature gradients that induce residual stresses on the printed component and can lead to part distortions during or after the component is removed from the building plate as the semi-solid filament returns to a solid state.

As a result, various printing factors, such as extrusion temperature, chamber temperature, nozzle velocity, and extruded filament diameters, along with thermal gradients, significantly affect the quality of the components produced. Experimental evidence has shown that these factors can impact the mechanical properties of the printed part, including yield strength, strain at failure, as well as its form and dimensions. Research institutions and businesses are increasingly interested in mechanical simulations to predict residual stresses and component deformation. Several research studies published in recent years have focused on predicting the mechanical behavior of FDM printed components[4].

Additive manufacturing allows for the production of complex shapes without the design limitations of traditional production techniques. Therefore, the focus of the design process shifts to the functional requirements of a component. However, additive manufacturing processes can pose certain challenges. The manufacturing process induces thermal strains, resulting in residual stresses that can cause part failure during manufacturing or while in use. One of the main goals of additive manufacturing simulation is to predict the remaining stresses in a component and minimize the difference between the manufactured part and the simulation prediction by optimizing the process. It also involves analyzing the performance of a manufactured part in an assembly with other parts under actual loading conditions.

2.3.1 AM-Modeler (AM-plugin)

First, a model to be simulated must be designed in CAD or within FE software. Second, describe material properties, boundary conditions, and thermal conditions in the model. Lastly, run the simulation. Abaqus has an advanced option for simulating additive manufacturing process which is called “AM Modeler plug-in” in which the simulation is solved in two different ways within Abaqus AM modeler, that is[5]:

- Eigenstrain
- Thermomechnical

For this particular project, the sequentially coupled thermo-mechanical analysis approach has been carried out. This means heat transfer analysis is performed first and then mechanical analysis is carried out, and the results of thermal analysis are introduced as a predefined field in the mechanical analysis. Thermal results are independent of the stress field but the mechanical results are dependent on thermal loads.

Process setup is an important factor in the process simulation where printing parameters such as nozzle temperature, layer thickness, and printing speed. The material flow behavior and deposition process are controlled by these parameters.

Inside the Abaqus FE analysis software suite, the AM modeler is a specialized tool made for simulating AM processes. It allows users to precisely model and analyze several AM process elements, including residual stresses, temperature effects, layer-by-layer material deposition, and material characteristics.

Three main features should be incorporated into the simulation for heat transfer analysis:

- Material Arrival: Over a period of time material is added incrementally.
- Heating: Once the material is added it gets heated to melt and combine with the below layers.
- Cooling: The cooling surface evolved with time as the part was printed.

For stress analysis:

- The temperature from thermal analysis is loaded as predefined in the stress analysis.
- Temperature-dependent material properties have to be used to capture the correct results.
- Over a period of time material is added incrementally

The first thing in the AM modeler is to set the data and there are three data types:

- **Event series:** In the AM process, the part is created in a layer-by-layer method, to capture this complex process within a brief period, the AM process can be defined by a finite series of events.
- **Parameter Table:** It is a list of process-specific parameters, not a function of time, space, or material state and it can be 'String', 'Integer','Float'or 'Enum'.

- **Property Table:** It defines dependent parameters, which could be dependent on temperature, and the number of field variables. Examples: Material properties, Film coefficient, and Absorptivity.

- **Table Collection:** Contains all the parameters table and property table specific to a particular event. The parameter and property tables are collected in a table collection that passes to the user subroutines.

2.3.2 Element Activation

In additive techniques, such as fusion deposition modeling, raw material is typically injected onto a platform through a nozzle. The nozzle uses the raw material to create the cross-section pattern for each layer. Materials are stacked layer by layer to complete the construction. Once the raw material has cooled down, it solidifies, even if it was once molten. The deposition of raw material from a moving nozzle is simulated in a progressive activation in a thermal or structural study. The complete definition of the deposition process involves the following steps: Simulating the deposition of raw material from a moving nozzle through progressive activation in thermal or structural analysis. Considering the material bead (single layer) being deposited and the cross-sectional area of the nozzle. To complete the deposition process, the following actions need to be followed[6]:

- Describe the nozzle's movement in an event sequence.

- Make a table collection with the name "ABQ_ AM" at the start. A parameter table of type "ABQ_AM_MaterialDeposition" and a parameter table of type "ABQ_AM_MaterialDeposition_Bead" must be present in the table collection.

- Add a reference to the nozzle motion event series in the parameter table of type "ABQ_AM_MaterialDeposition" and choose "Bead" as the deposition process type.

- In the parameter table of type "ABQ_AM_MaterialDeposition_Bead", define the process parameters, such as the height and width of the bead.

- Refer to the table collection in the progressive element activation.

AM is a continuous process of depositing new layers of material and to activate the elements it can be done in two ways, one is quiet elements and another is inactive elements. [7][8]. In this thesis work, the inactive element technique is employed. The elements of the deposited material are not included in the model before the material is added, which is known as the inactive element method. To determine which elements should be triggered at the current time step, a control volume is used in the thermal analysis. The mechanical activation in temperature-displacement analysis is determined by temperature. When the average temperature of an element falls below its melting point, the element is said to be activated.

The activation of the element is done in each increment of the step. At the beginning

of each increment, the elements are activated by giving a volume fraction of the material. There are two supported ways for element activation either full or partial. To have a full activation the volume fraction of material must either be 0 or 1, however, the volume fraction of material can be arbitrary for the partial activation[9].

3 METHOD

The steps taken to obtain results are explained in the flowchart depicted in Figure 4. The flowchart provides a structured overview of the sequential actions followed in the methodology, from the initial stages of data preparation to the final analysis.

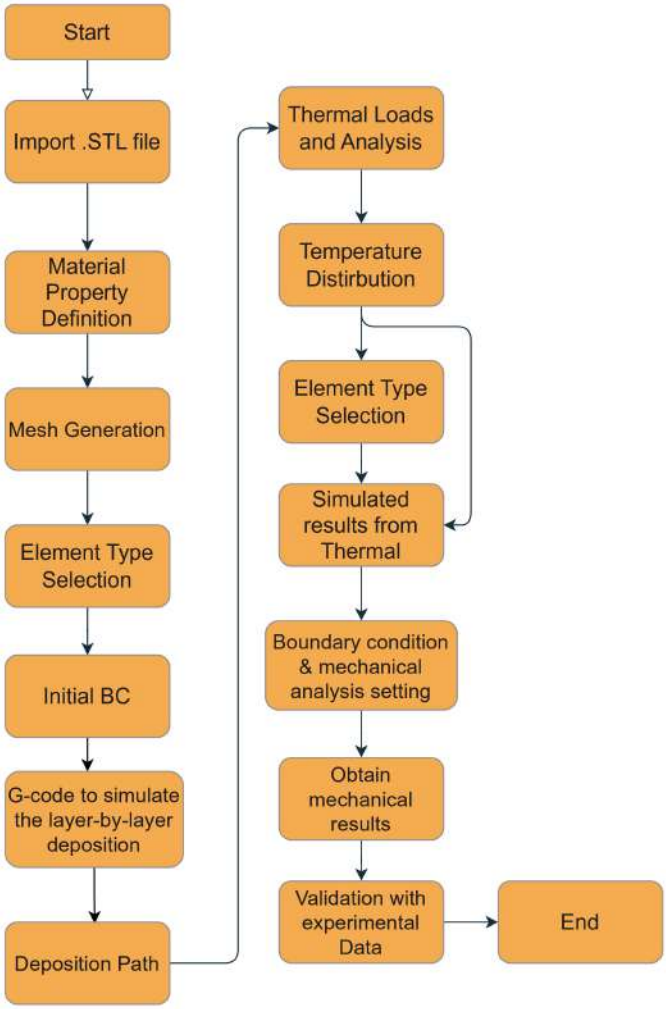

Figure 4: Flowchart outlines the steps used in the project

Simulation in Abaqus involves several steps to accurately model the layer-by-layer deposition process. It begins with importing the STL file, which represents the geometry of the part to be manufactured.First, CAD software is used to create a model of the part. Then, a mesh of the exterior surface is created (STL file) and used as input to provide all the parameters needed for the printing process, such as filament deposition path, deposition speed, extrusion temperature, and environmental factors, using slicing software. All this information is stored in a file called GCode, which is used to simulate the component and carry out the printing process.

After importing the geometry, material properties are defined in Abaqus to capture

the thermal and mechanical behavior of the polymer throughout the process. The next step involves creating a finite element mesh based on the imported geometry. During simulation, the elements will be activated piece by piece to enable detailed analysis. Selecting the appropriate type of element is crucial at this stage, as it determines whether the model accurately captures the physical phenomena being addressed, whether they are thermal, mechanical, or both.

The initial boundary conditions are applied to the model, including constraints and initial temperatures, to set the stage for the simulation to proceed. The G-code, containing specific instructions for layer-by-layer deposition, is input into the AM modeler to control the sequential activation of elements within the mesh. This simulation represents the actual deposition path followed by the 3D printer to build the model layer by layer. Thermal loads are applied to the model to simulate the heat input during deposition, and a thermal analysis is conducted to understand the resulting temperature distribution across the part. Understanding this temperature distribution is crucial, as it controls the part's subsequent mechanical behavior. The element type is then re-evaluated to ensure its effectiveness for post-mechanical analysis.

Boundaries and settings are adjusted to simulate the part's behavior in terms of stress distribution and deformation. The mechanical analysis is carried out to gain insight into the structural integrity after the part is manufactured. The simulation results are verified by comparing them to experimental data to ensure that the simulated behavior matches the real part after manufacture. This methodological approach provides a deep understanding of the additive manufacturing process and its effects on the final product.

An FE model was developed in Abaqus (v. 2021) using a sequential element activation strategy to simulate the complete printing process. The analysis consists of two phases. First, a thermal analysis using the heat equation is conducted to assess the time-spatial temperature field evolution throughout the sequential element activation process. The resulting temperature field is then used as a forcing factor in a mechanical study to assess residual stresses and part deformation.

A Python code was created as a custom G-Code reader for specific configurations such as computer numerical control (CNC) or 3D printing. This code is designed to analyze G-codes that control materials and movement in machines to extract relevant information for further action or study. The code includes imported modules and customer support classes for data handling and regular expressions. It also features constant declarations, global variables, and helper functions for extracting parameters through regular expressions based on input text lists. The program's activities are coordinated within a function called CreateLayers. This function opens G-code files and processes the movements according to the standard syntax. For additive manufacturing or 3D printing, a Python script is essential as it generates G-code instructions for the proper placement of materials and the use of predetermined strategies. To enable the software program to perform its functions in a pre-configured environment, the script loads all modules first and then determines

global variables. The CreateLayers function reads the G-code file, generates material deposition layers according to stipulated guidelines, creates corresponding path points, computes deposition widths, and takes care of motion states, among other tasks. Additionally, the script controls the extruder's heating element, and roller activation, and adjusts time and coordinates to correspond to user-defined intervals within which the additive manufacturing (AM) procedure can be effectively managed.[4].

3.1 Material Properties

It is crucial to accurately represent material characteristics because they have a significant impact on temperature changes and the mechanical behavior of an object. These properties often vary with temperature, which must be taken into consideration. The inclusion of temperature-dependent characteristics such as conductivity, specific heat capacity, density, and emissivity introduces non-linearity into the solution. These features are essential for accurately representing the behavior of the system.

For simulating additive manufacturing (AM) of polymers like nylon 6, 30% mineral filled, precise material modeling is necessary to understand the mechanical and thermal behavior of printed parts. Abaqus offers sophisticated systems for material modeling. Engineers and researchers can use established equations and relationships that utilize the provided property information to accurately model the AM process for Nylon 6, 30% mineral filled, improve system design, and estimate component performance.

Nylon 6, 30% mineral filled, is a composite material that combines nylon 6, a synthetic polymer, with mineral fillers for printing parts. This material is widely used in various industries, including automotive, consumer products, and electronics, due to its excellent mechanical properties and toughness when combined with minerals. The bed material for depositing the Nylon 6 composite is PEI (polyetherimide) aluminum coated. In our project overview, mentioned that the material is obtained from recycling ocean fish nets to create a usable product. However, it's important to note that comprehensive testing specific to our material was not achieved within the scope of this project. To address this gap, utilized existing literature [10] and online resources to gather relevant data, although it may not perfectly reflect our material. Based on the available data, we will set up an initial simulation and refine parameters as the project progresses to obtain accurate results. This approach will allow us to preview the material's behavior under different conditions and validate our findings. The model initiation properties used are detailed in Table 1 and Table 2 serving as our starting points for the modeling process.

Conductivity,k	0.00031 W/mmK
Young's modulus, E	4580 MPa
Poisson's ratio, ν	0.3
Expansion, α	8.9×10^{-5} mm/mm$^{\circ}C$
Specific Heat, c	$2 \times 10^{6}\ mm^2/s^2K$
Density, ρ	$1.37 \times 10^{-9}\ Tonne/mm^3$

Table 1: Thermal and mechanical properties of the Nylon6 30% mineral filled

Conductivity,k	0.000327 W/mmK
Young's modulus, E	8000 MPa
Poisson's ratio, ν	0.37
Expansion, α	2×10^{-5} mm/mm$^{\circ}C$
Specific Heat, c	$5 \times 10^{9}\ mm^2/s^2K$
Density, ρ	$2 \times 10^{-9}\ Tonne/mm^3$

Table 2: Thermal and mechanical properties of the PEI, Aluminum coated

3.2 Thermal Model Description

The following conditions must be met to create a simulation model for the FDM process: Resolving the issue of transient heat transfer, simulating the insertion of material, taking heat losses during deposition into consideration, and taking temperature-dependent material characteristics into account. The energy conservation principle, which asserts that the difference between heat production in the volume and the heat flow over the boundary surface is equal to the energy fluctuation in a volume over some time, provides the foundation for the formulation of the transient thermal issue [11][8]. This may be represented as for a very small volume as

$$\frac{\partial U}{\partial t} = -\nabla \cdot \underset{\sim}{q} + q_{gen} \tag{1}$$

where $\underset{\sim}{q}$ is the heat flux density vector, q_{gen} is the rate of heat production density, and $\tilde{U}$ is the specific internal energy rate. Furthermore, the constitute equation shows that Fourier's law links temperature and heat flux

$$\underset{\sim}{q} = -k\nabla T \tag{2}$$

where k is the thermal conductivity and T the is temperature. The constitute equation defines the connection between the specific internal energy U and temperature T

$$U = U_o + \rho c T \tag{3}$$

where c is the material's specific heat capacity and ρ is its mass density. The partial differential equation for the thermal process is as follows

$$\rho c \frac{\partial T}{\partial t} = \nabla \cdot (k \nabla T) + q_{gen} \tag{4}$$

Here, assuming no heat source which implies that no additional internal heat is generated within the material, hence, $q_{gen} = 0$. As a result, the heat transfer depends entirely on the initial temperature distribution and heat flux across the boundaries of the material. Regarding hot extruders that produce high levels of heat and impact material temperature, the internal heat generation factor is not included in the thermal model. This simplification means that when calculating the temperature distribution, only heat conduction caused by temperature gradients and boundary conditions like ambient temperature or heat flux at the surface is taken into account.

This is the mathematical model's strong form, which must be solved to determine the temperature's temporal history. Since an analytical or closed solution is not feasible, this study will employ the numerical solution or FE simulation. Using the conventional Galerkin approach with finite elements, the thermal model is first discretized in space. It is fine for the temperature to change throughout time and space. This dependency is divided for each element using the interpolation model.

$$T(x, y, z, t) = T(x_1, x_2, x_3, t) = [N(x_1, y_2, z_3)]^T \, T_e(t) \tag{5}$$

Where, $[N(x_1, y_2, z_3)]^T$ is the transpose matrix of the element shape function and $T_e(t)$ is the vector of the nodal temperatures.
The system of differential equations is expressed by:

$$[C]\{\dot{T}\} + [K]\{T\} = \{Q\} \tag{6}$$

Where, C is the specific heat matrix, T is the nodal vector of temperature,$\dot{T}$ is the rate of change of temperature, K is the conductivity and Q is the heat flow vector. Every time step of the discretization of time results in an algebraic equation system that can be solved for the unknown nodal temperatures. The temperature field's numerical representation is given by the FE equations solution. The adhesion behavior between the filaments may be predicted by combining the bonding potential model with the temporal history of temperature at a place in space. Additionally, using the definition, the phase change problem may be solved by determining the particular heat matrix from the enthalpy curve:

$$H = \int_{T}^{T_0} \rho(T) \; c(T) \; dT \tag{7}$$

The filament is extruded at temperature T_n during the FDM process and deposited on the construction bed D_b, which is heated to T_b. The temperature T_c is maintained constant within the construction chamber D_c. The filaments exchange thermal

energy with the air in the chamber as well as the material that was previously deposited because of temperature gradients following equation (4).

$$\rho c\dot{T} = \nabla.(k\nabla T) + q_{gen} \tag{8}$$

This well-known heat equation, where $\rho = \rho(T)$ is the material density, $c = c(T)$ is the specific heat capacity, $k = k(T)$ is the thermal conductivity, $q_{gen} = 0$ is the internal heat source, and t is the time, controls the temporal-spatial development of the temperature field T(x,t). The problem's starting circumstances are provided by

$$T(x, 0) = T_n \qquad x \in D_f \tag{9}$$

$$T(x, 0) = T_c \qquad x \in D_c \tag{10}$$

where x represents the position vector (x, y, z), D_f denotes the extruded deposited material, T_n and T_c refer to the extrusion temperature and the chamber temperature of the building chamber. The essence of a Dirichlet boundary condition is to indicate what the solution function is worth at given locations along the boundary of a region. Typically these are fixed by considerations of physicality or experiment. Thus, the Neumann boundary condition specifies:

$$T(x, t) = T_b \qquad x \in D_b \tag{11}$$

One method is to impose such boundary conditions on a solution function by specifying how it changes at the edge of the region where they apply:

$$k\frac{\partial T}{\partial n} + q_c + q_r = 0 \qquad x \in S(t) \tag{12}$$

where S(t) represents the outer surface of the object n is the perpendicular vector to the q_c and q_r refers to the heat fluxes caused by convection and on the outer layer of the body radiation, defined as

$$q_c = h(T - T_c) \tag{13}$$

$$q_r = K_b(T^4 - T_c^4)\epsilon \tag{14}$$

where h=h(T) is the heat transfer coefficient, K_b represents the Stefan-Boltzmann constant, and ϵ is emissivity.

3.3 Mechanical Model Description

The simulation shown here shows a part made with a 30% mineral filled which behaves like a conventional thermo-plastic [12][8]. The additive decompositon of strain is often included in incremental plasticity theory, under the assumption of a small strain regime.

$$\boldsymbol{\epsilon} = \boldsymbol{\epsilon}^e + \boldsymbol{\epsilon}^p + \boldsymbol{\epsilon}^T \tag{15}$$

Where, $\boldsymbol{\epsilon}$ is the total strain, $\boldsymbol{\epsilon}^e$ elastic strain, $\boldsymbol{\epsilon}^p$ is the plastic strain and $\boldsymbol{\epsilon}^T$ is the thermal strain tensors. These can be expressed using Voigt notation:

$$\boldsymbol{\epsilon}^e = \boldsymbol{D^{-1}\sigma} \tag{16}$$

$$d\boldsymbol{\epsilon}^p = d\lambda \frac{3}{2} \frac{\boldsymbol{\sigma}^{dev}}{\sigma_{\text{vm}}} \tag{17}$$

$$f(\sigma) = \sqrt{3J_2} - \sigma_Y \tag{18}$$

$$\boldsymbol{\epsilon}^T = \alpha(T - T_o)\mathbf{1} \tag{19}$$

where $\boldsymbol{\sigma}$ is the stress, where J_2 is the second invariant of the deviatoric stress tensor, and σ_Y is the yield stress, α is the thermal expansion, $\mathbf{1} = \{1, 1, 1, 0, 0, 0\}^T$ and finally $\boldsymbol{\sigma^{dev}}$ is the deviatoric stress

$$\boldsymbol{\sigma}^{dev} = \boldsymbol{\sigma} - \frac{1}{3} tr\boldsymbol{\sigma}\mathbf{1} \tag{20}$$

The plastic flow factor or $d\lambda$, is described as follows:

$$d\lambda = 0 \qquad if \qquad \sigma_{vm} < \sigma_p \tag{21}$$

$$d\lambda > 0 \qquad if \qquad \sigma_{vm} > \sigma_p \tag{22}$$

where σ_p is the yield stress and σ_{vm} is the equivalent von Mises stress defined as:

$$\sigma_{vm} = \sqrt{\frac{3}{2}(\boldsymbol{\sigma}^{dev})^T \boldsymbol{\sigma}^{dev}} \tag{23}$$

3.4 Model Setup

The main focus of this study will be the Eel lounge chair, as shown in Figure 5. This chair is to be evaluated and simulated in relation to the AM printing process using Abaqus. Abaqus CAE, a commercial finite element modeling and simulation package, was used for simulations to determine the behavior of the models under required loading conditions. An average mesh size of 5 mm, was used to achieve the ideal balance between computational costs, efficiency, and accuracy. The conventional 3D stress analysis, 8-node linear brick finite elements, reduced integration, and default hourglass control were used to design and mesh the 3D portion.

For the thermal analysis 8-node linear brick, reduced integration, with the hourglass control element DC3DR is been implemented and for stress analysis 8-node linear brick, reduced integration with the hourglass control element CD3DR is used from the Abaqus library. The model has a total number of linear hexahedron elements: 173800 and a total number of nodes: 221595.

A material model was developed to accurately simulate the behavior of a material nylon PA6. This model considers a wide range of parameters such as mechanical property, thermal behavior, etc that are important in understanding the material behavior during AM. With a view to FDM simulation the considerations for modeling that were presented in Section 2.3 have been implemented. The final model created including factors in Section 2.3 is shown in Figure 5.

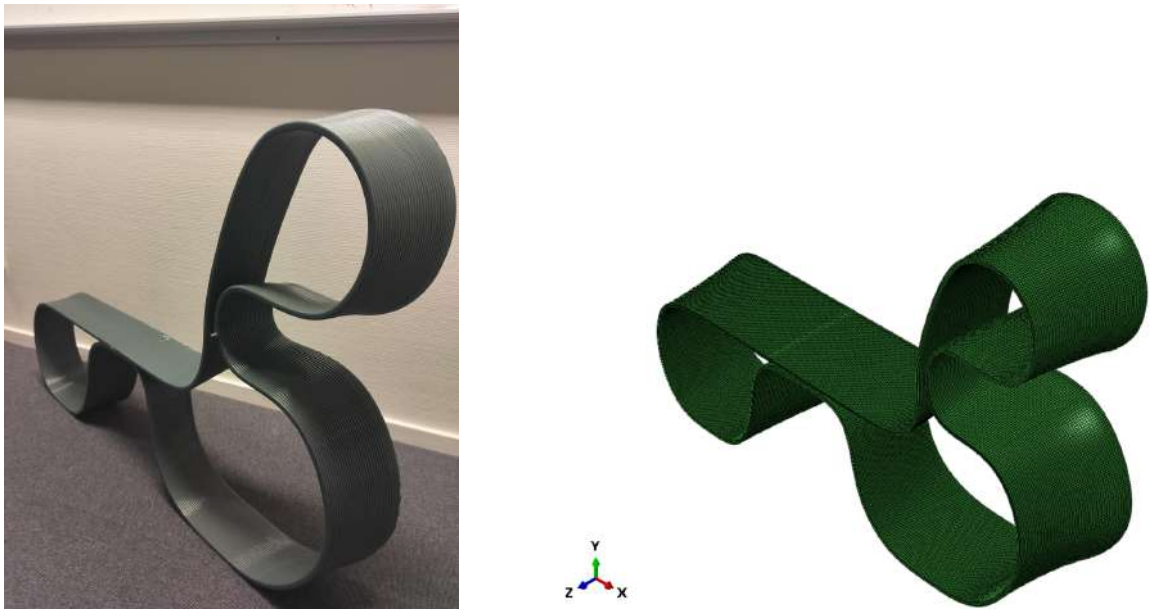

(a) (b)

Figure 5: Eel Lounge chair and Numerical model FE Mesh

3.5 Boundary Condition

The Boundary Conditions (BC) are crucial for the process model. The thermal and mechanical models have different boundary conditions. In the thermal model, a preheating temperature of 110 $°C$ was applied to the bed surface where the material is being deposited. Preheating the build plate reduces residual stresses at the bottom of the part and enhances the material's mechanical properties [13]. A constant temperature of 225 $°C$ is applied to the entire part during the heat transfer analysis, as the material through the nozzle is being deposited at the same temperature. This ensures realistic temperature distributions throughout the material and accounts for the thermal conditions encountered during the AM process. A controlled sink temperature of 42 $°C$ was maintained within the printing chamber. This temperature control is crucial to ensure a stable environment during the printing process, which helps prevent possible adverse effects of thermal fluctuation on the quality and consistency of the printed parts. This minimizes the possibility of thermal stresses and material deformation, allowing for improved mechanical properties and dimensional accuracy. The results of the thermal analysis are then used as a predefined field in the mechanical analysis, taking into account thermal expansion effects and temperature-dependent material properties found in the heat transfer study.

In the mechanical model, the main boundary condition is a fixed constraint applied to the bottom of the bed. To prevent distortions unrelated to the printing process, all three displacement degrees of freedom are set to zero. Additionally, the transient thermal temperature field obtained from the heat transfer study is applied to the entire model. The thesis focused on improving and implementing these boundary conditions. While the bottom of the printed object is often completely restricted in simulations, this fixation does not accurately represent real-world conditions. It is crucial to create realistic boundary conditions in order to accurately capture genuine distortion in the part.

3.6 Interactions

In this section, the interactions used to model heat transfer and mechanical analysis will be clearly defined. Following that, a detailed explanation will be provided on how these interactions will be featured within the FE model to ensure that the thermal and mechanical behaviors are properly captured.

3.6.1 Interactions for thermal analysis

In this section, we model the interaction between the bed and the part. The thermal model establishes a surface-to-surface contact between the two areas. First, contact is made at the two adjacent surfaces, as shown in Figure 6. Second, contact is made between the bed and the bottom of the part, as shown in Figure 7. Additionally, a surface film condition is implemented for the inner and outer surfaces of the part during the analysis.

GAP Conductance: In this thesis, one of the main focuses is on modeling thermal gap conductance. The heat transmission between two adjacent surfaces in the model is simulated using a gap conductance model. Despite recent advancements in research on heat transfer between two surfaces, thermal gap conductance models are rarely taken into account in the finite element analysis of additive manufacturing for polymers. There are three types of thermal conductance: radiation, heat generation, and conductance. Heat transfer between surfaces that is conductive is referred to as gap conductance; heat transfer between surfaces that is caused by a small gap is referred to as gap radiation; and heat created by friction is referred to as gap heat generation. There are three methods to define gap conductance: using only clearance-dependency data, using only pressure-dependency data, or integrating both clearance and pressure-dependency data. This study exclusively used clearance-dependent data. If gap conductance is defined as a function of clearance, then the conductance value drops to zero when clearance exceeds the corresponding data point value.

In the FE modeling, the contact is defined between the slave surface and the master surface. Heat transmission between two surfaces in contact can only be achieved by specifying the gap conductance coefficient using the finite element method. Implementing gap conductance is crucial for accurately modeling heat transfer between close surfaces. The outcomes of the heat and stress analyses are greatly impacted

by this. The first important region is the space between two adjacent surfaces, as shown in Figure 6. The second key area is between the bed and the lounge chair (part), which is also shown in Figure 7. To ensure precision in the entire study, gap conductance in these places needs to be accurately taken into consideration. The gap between two adjacent surfaces varies from 2 mm at the center to 35 mm towards both the right and left sides. Three different gap conductance theoretical models have been implemented so far to determine which model yields the most accurate findings. The model that gave the closest results is represented here, and the remaining two models are described in the following section 7.2

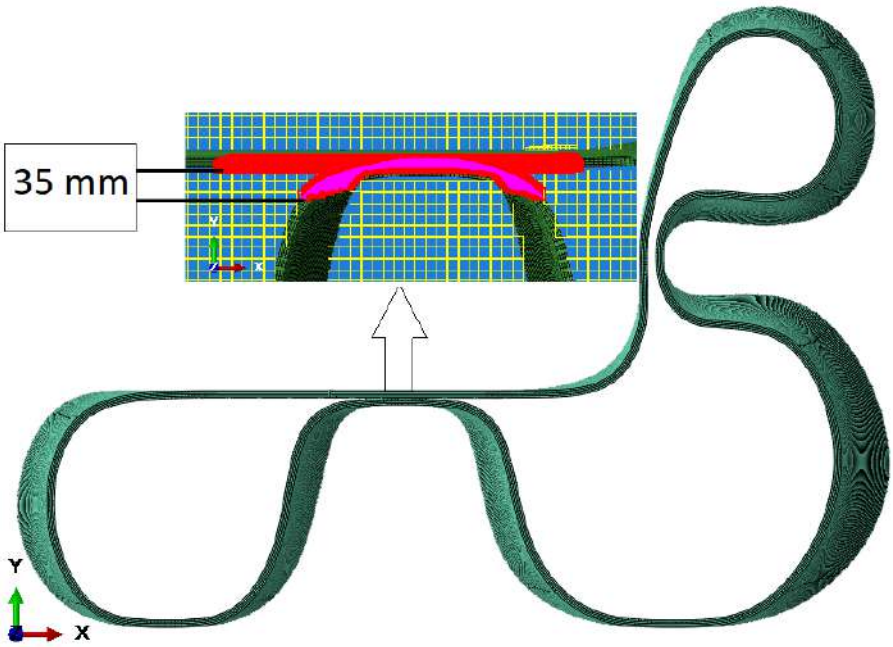

Figure 6: Shows implementation of contact and Gap conductance between adjacent surfaces

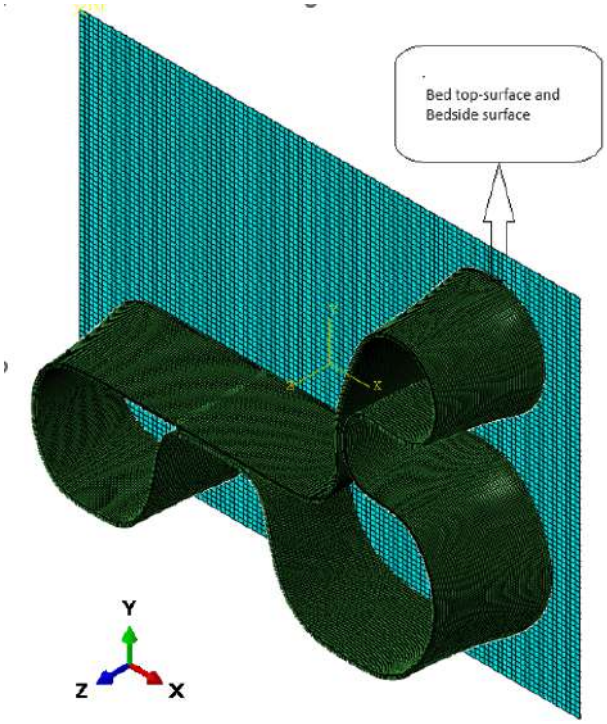

Figure 7: Shows implementation of contact and Gap conductance between bed and part

The gap conductance equation is derived from Abaqus documentation and is defined below [14].

$$q = K(\theta_A - \theta_B) \tag{24}$$

q represents the heat flux per unit area moving between points A and B on a surface, with K as the coefficient for gap conductance and θ_A and θ_B are the surface temperatures. The calculation of heat flux involves:

$$q = k\frac{\Delta T}{d} \tag{25}$$

where k is the thermal conductivity of the material, and ΔT is the difference in the temperature. Here, k represents the conductance, that is, the ability of the heat to flow across the gap. It can be defined as a function of either the gap clearance, d, or the contact pressure, p. If the gap conductance, k, is defined by Abaqus as a function of clearance, d, it will calculate the heat transfer based on how far the two surfaces are apart. This relationship is often not linear, as the diagram provided shows in Figure 8 [14]. The diagram indicates that for any increase in the clearance, d, there is a decrease in conductance, k.

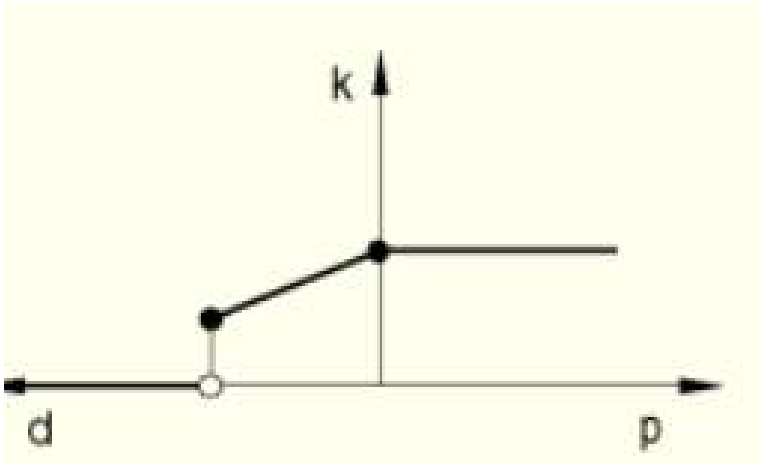

Figure 8: Defining gap conductance as a function of clearance

Under conditions of zero clearance, where the surfaces are fully in contact, the conductance k would be maximum. This is the highest possible heat transfer condition because the gap between the surfaces is nonexistent. The conductance increases as the gap d between them decreases and also when k drops. Enlarging gaps reduces the efficiency of heat transfer because a small percentage of physical conduction can occur through contact.

It defines a plot of a clearance d beyond which conductance k falls instantly to zero. The critical clearance is the maximum value that may be defined by the user in the input data. Abaqus will after this point operate on the assumption that no heat transfer will occur between the surfaces as a consequence of them being too far apart.

Unless the gap conductance is also user-defined as a function of contact pressure, Abaqus will assume that remains constant at the value associated with zero clearance, regardless of how the contact pressure changes. This means the conductance will not change once the surfaces are in contact, or the clearance is zero, even if the pressure applied to the surfaces varies. The approach will allow modeling, in any complexity, the realistic thermal interaction between components within a finite element model when the gap between contacting surfaces influences the efficiency of heat transfer.

3.6.2 Interactions in mechanical analysis

Spring elements were used to simulate the interaction at the bottom nodes of the part with the ground (bed) in the mechanical analysis as shown in Figure 9. These springs were crucial in modeling the structural response under various loading conditions. The spring elements were set up and configured in Abaqus to generate a better representation of the mechanical behavior of the system. The spring elements were defined with the "Connect points to ground (Standard)". The springs were then applied to a region, which was more important, the bottom nodes of the part being analyzed. The region was important in ensuring that the springs were attached

to the right nodes of the model to provide the correct constraints that introduce stiffness to simulate the mechanical response.

In this case, degrees of freedom (DOFs) were selected as 1 and 2, which relate to the global directions of X and Y, respectively. As shown in Figure 9(a) refers to the configuration for spring elements with DOF 1 along the X-axis, while Figure 9(b) shows the configuration for DOF 2 along the Y-axis. This means that the relative displacement across each element of SPRING1 is measured on these two axes.

- DOF 1 (X-axis): The relative displacement of the node in the global X direction.
- DOF 2 (Y-axis): The relative displacement of the node in the global Y direction.

$$\Delta u = u_i \tag{26}$$

The relative displacement is the amplitude of movement of the node of the spring in a particular direction and is denoted by i. The direction i can be either in the global coordinate system or in some locally defined coordinate system.

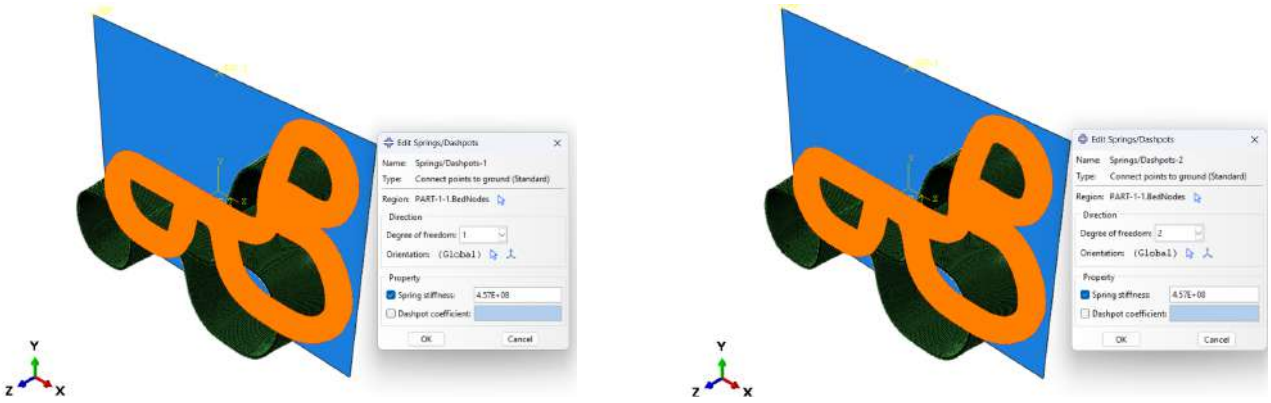

(a) (b)

Figure 9: Spring element configurations for the part-ground interaction in Abaqus, with DOF 1 (a) along the X-axis and DOF 2 (b) along the Y-axis

These movements hold great significance as they determine the amount of force that will eventually be produced by the spring components. The SPRING1 element takes this displacement at the node and converts it into a respective force by utilization of the stiffness value that has been assigned in the property section. If a node shifts along the X-axis, the displacement recorded by DOF 1 will cause a force in that same direction, which is directly related to the displacement and stiffness value that is assigned.

Because the setup involves both the X and Y directions, the springs can offer resistance to movement in these two directions, providing stability to the structure concerning displacement in the model's plane. This configuration with two axes is

highly beneficial in situations where precise control of nodal movements is necessary to guarantee the stability of the framework and precision of the simulation.

4 RESULTS

The results present the findings of the simulations carried out using the FDM method. These models include thermal and mechanical analyses that have been validated against experimental data. The findings offer important insights into the thermal dynamics and distortion caused by the thermal load during the printing process.

4.1 Results of Thermal Analysis

In this section, the analysis focuses on understanding the temperature change throughout the FDM simulation. Figure 10 depicts the temperature distribution during the initial stage, showing the temperature of the material after the nozzle exit at 225 $°C$, and Figure 11 shows the temperature distribution in an intermediate stage where the previous layers exhibit lower temperature due to heat dissipation. Finally, Figure 12 shows the temperature distribution at the final stage, after the complete deposition of material and the cooling period.

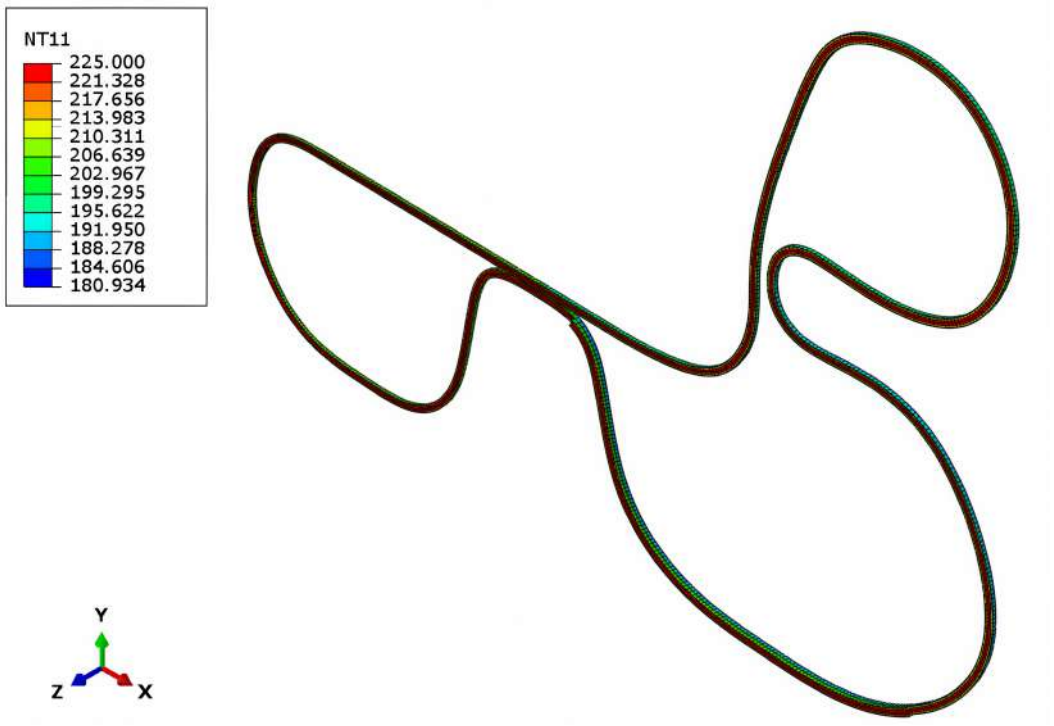

Figure 10: Temperature distribution at initial stage

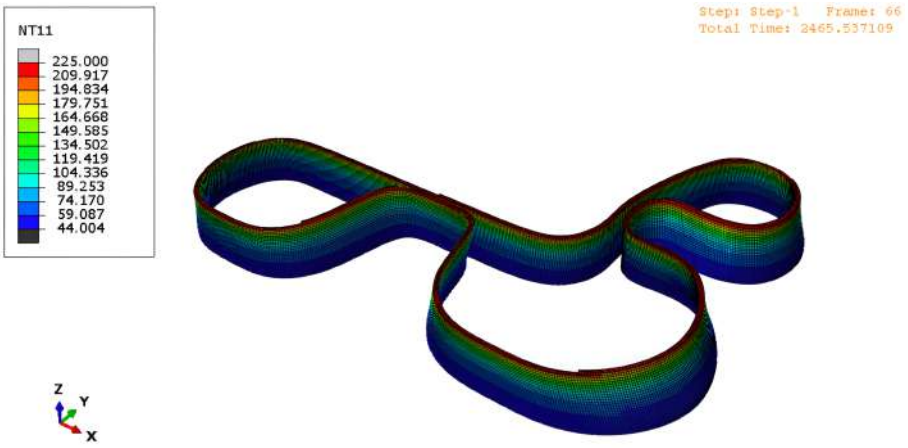

Figure 11: Temperature distribution at intermediate stage

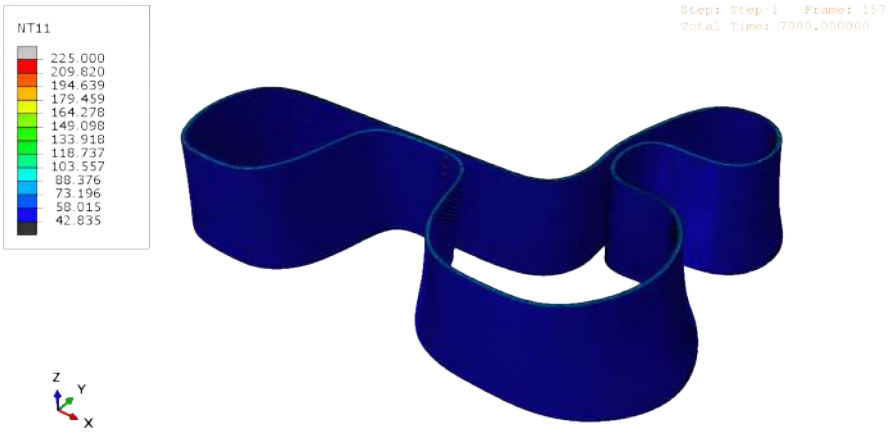

Figure 12: Temperature distribution at final stage

4.1.1 Temperature Evolution at Specific Points

The two integrated sensors have been positioned at two distinct spots: T1 and T2 to monitor changes in temperature during the printing process while collecting data for the simulation model. The position of the sensor T1 and sensor T2 can be observed in Figure 13. The locations of these sensors were very carefully selected to capture key thermal data.

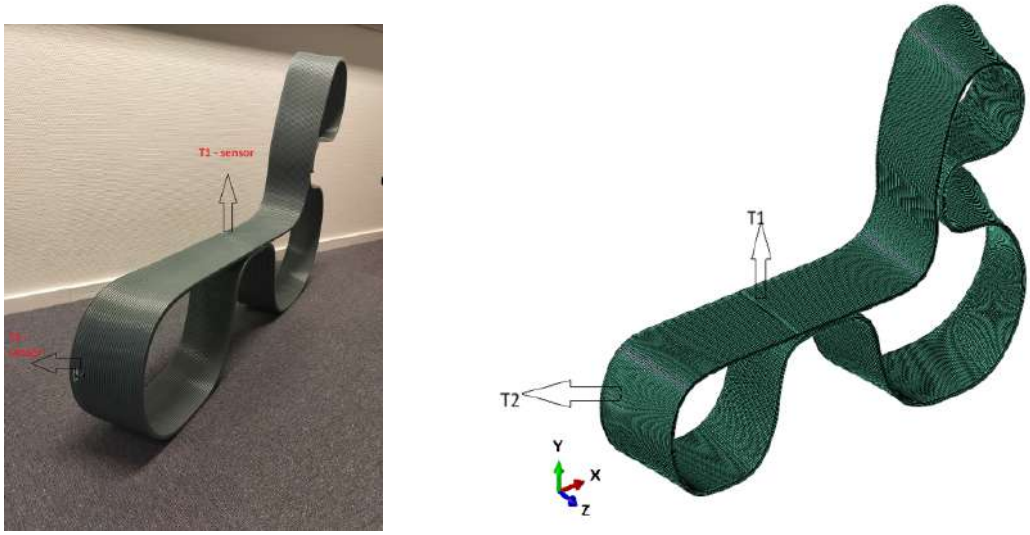

(a) (b)

Figure 13: Positions of the T1 and T2 sensors

Here the comparison is between the initial results of the model and the final results of the model to the experimental data.

Initial results: The initial results of simulation showed the following temperature evolution at sensor T1 and sensor T2 as shown in Figure 14 and Figure 15 respectively. The printing process is completed approximately at 4600 seconds which is indicated by the last green dot in the plot where the temperature stabilizes.

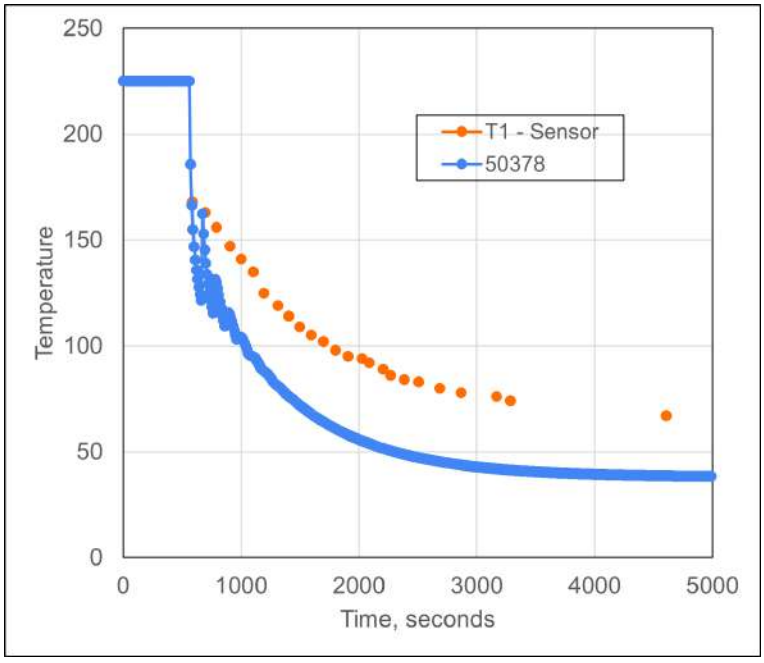

Figure 14: Initial results comparison at T1-sensor

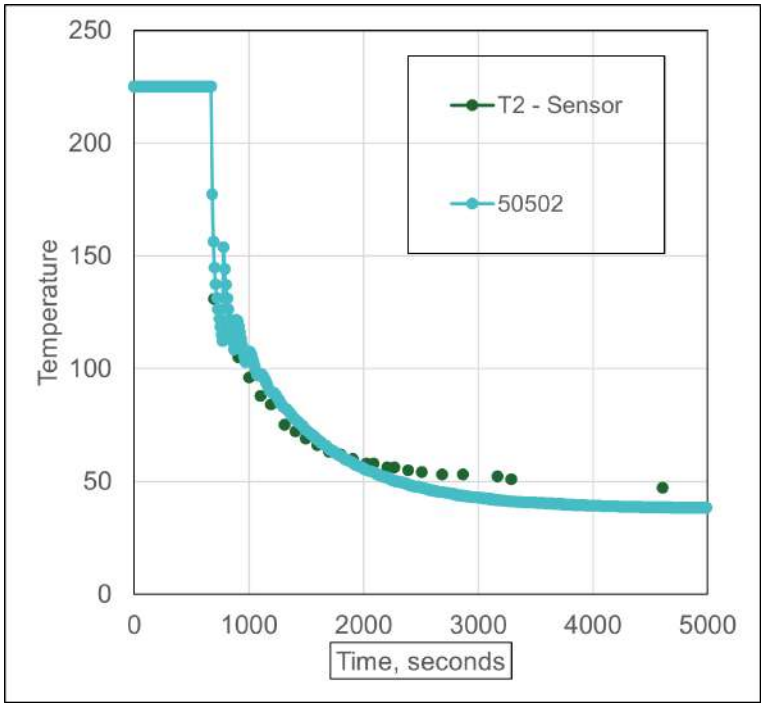

Figure 15: Initial results comparison at T2-sensor

Intermediate results: The intermediate results of the simulation follow the differences in the initial results of the T1 sensor. The introduction of gap conductance results in a slight improvement in the results as shown in Figures 18 and Figure 19.

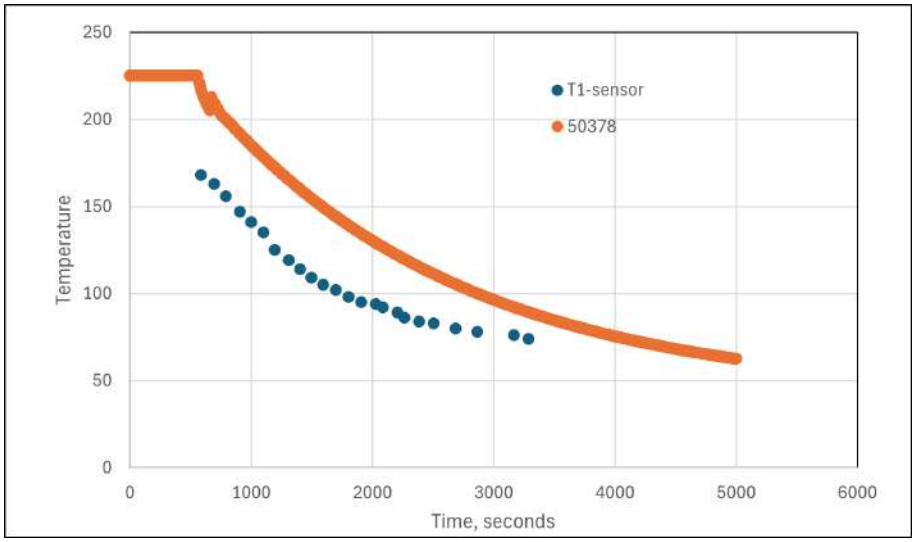

Figure 16: Results comparison at T1-sensor after implementing gap conductance

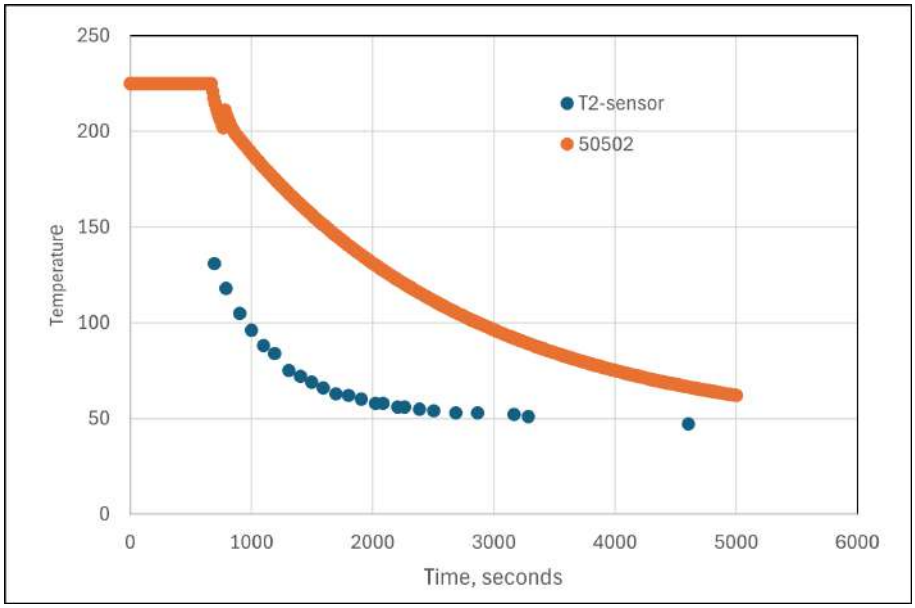

Figure 17: Results comparison at T2-sensor after implementing gap conductance

Final results: Further modifications had been made to the simulation following the differences in the intermediate results. Along with addition of gap conductance, the material parameter identification, h= 2.5×10^{-3} results as shown in Figure 18 and Figure 19, film coefficient, h= 4.5×10^{-3}, became one noticeable enhancement as shown in the Figure 20 and Figure 21 respectively.

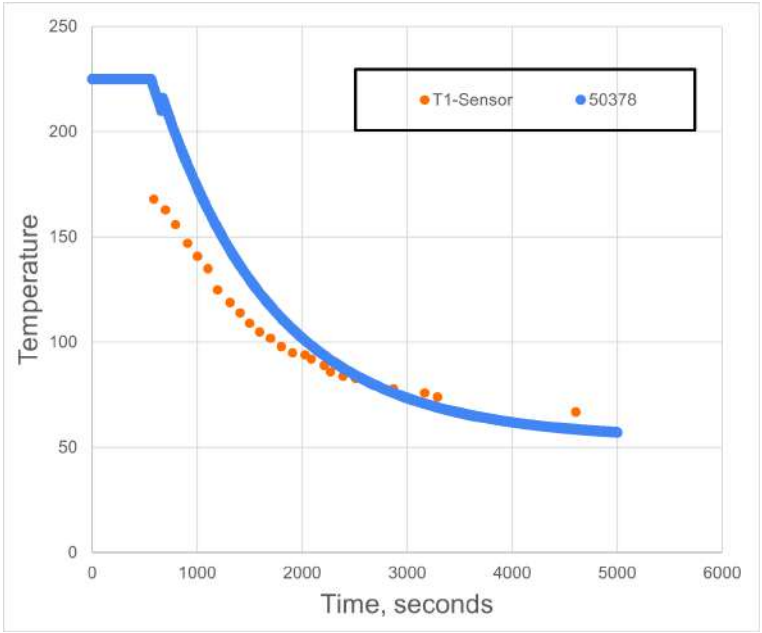

Figure 18: Results comparison at T1-sensor with implementation of gap conductance and film coefficient, h= 2.5×10^{-3}

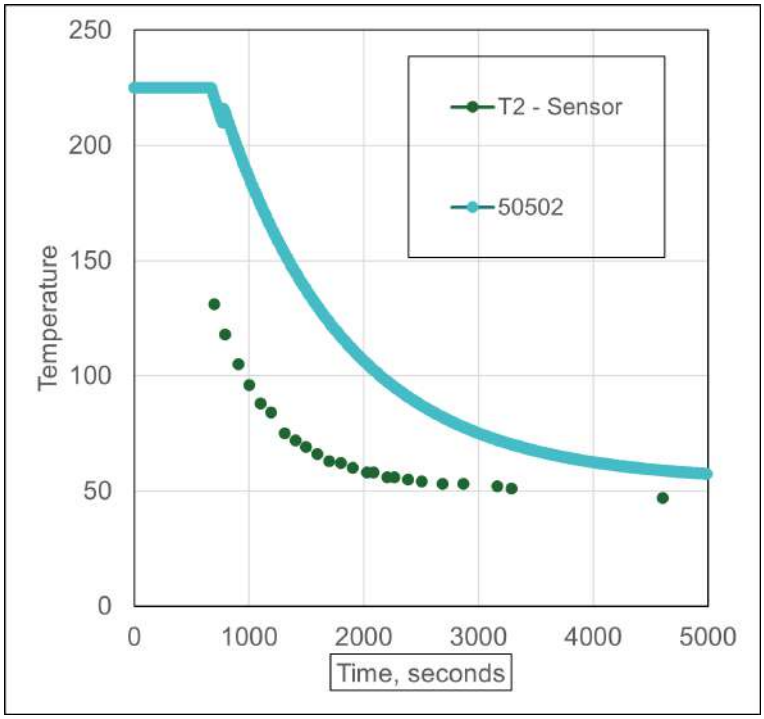

Figure 19: Results comparison at T2-sensor with implementation of gap conductance and film coefficient, h= 2.5×10^{-3}

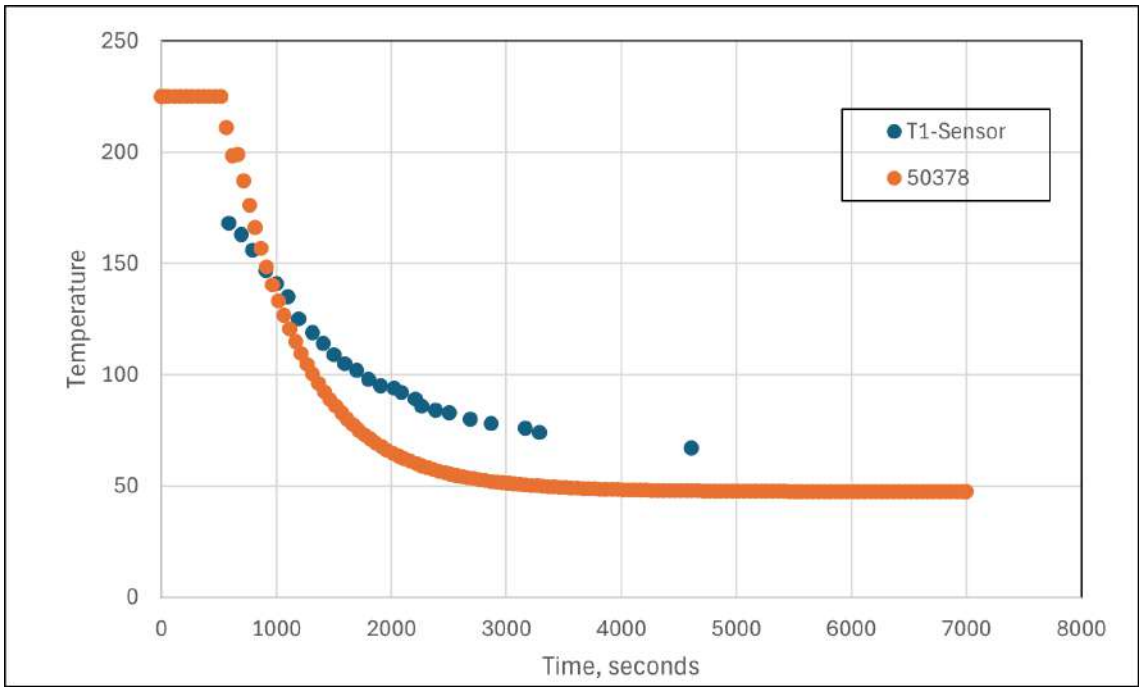

Figure 20: Results comparison at T1-sensor with implementation of gap conductance and film coefficient, h= 4.5×10^{-3}

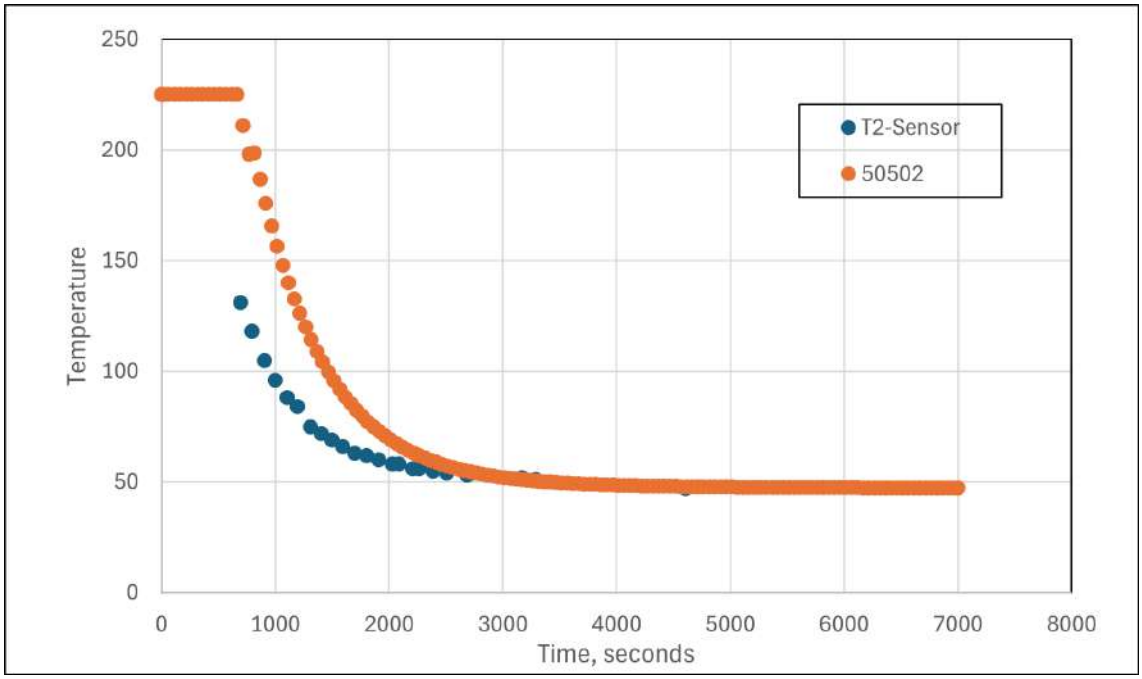

Figure 21: Results comparison at T2-sensor with implementation of gap conductance and film coefficient, h= 4.5×10^{-3}

4.2 Results of Mechanical Analysis

4.2.1 Comparison of Boundary Condition Cases

The thermal simulation results were used as input for a mechanical analysis. This analysis predicted the deformations caused by heat by mapping the temperature distribution over time onto the mechanical model. The goal was to assess how material expansion would affect the geometry of the component. The study considered various boundary conditions and loads to understand how these factors impact the mechanical behavior of the printed parts, particularly how they affect deformation and stress distribution.

Case-1: In this case, the translation in the Z direction was unrestricted, while the edges of the bed node were constrained in the U1 and U2 directions, allowing only vertical movement. Through an iterative process, the boundary conditions were adjusted to find the most accurate constraints that mimic the actual behavior of the part in the additive manufacturing process. Since applied loading was allowed, translation along the Z-axis was permitted, potentially resulting in significant out-of-plane deformations. In the X and Y directions, restrictions were imposed to prohibit transverse displacements, but non-uniform deformation might occur due to the limited control of stiffness in the Z direction as shown in Figure 22.

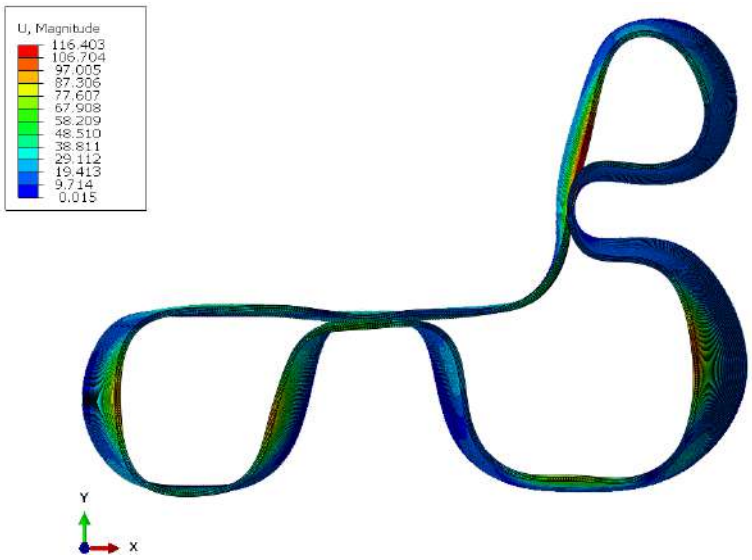

Figure 22: Deformation for case-1

Case-2: The bottom of the part was secured to the ground using a spring restraint that was fixed in both the X and Y directions. All DOFs for the bed were restricted, and the spring had a stiffness of 4570 N/mm. A lower spring stiffness provided better resistance to deformation, especially in the Z direction. This setup might have made the bed more flexible, leading to increased displacements under load. However, restraining all DOFs provided some stability but did not effectively prevent vertical movement, as illustrated in Figure 23.

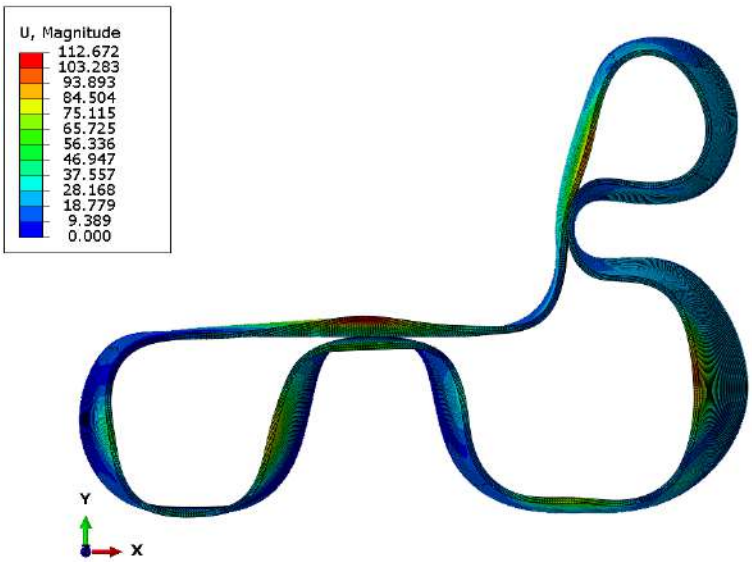

Figure 23: Deformation for case-2

Case-3: The bed was treated as a rigid body, and the bottom of the part was fixed to the ground using a spring constraint that was anchored in the X and Y axes.

The stiffness of the spring was significantly increased to 457000 N/mm. However, defining the bed as a rigid body led to poor output, as depicted in Figure 24.

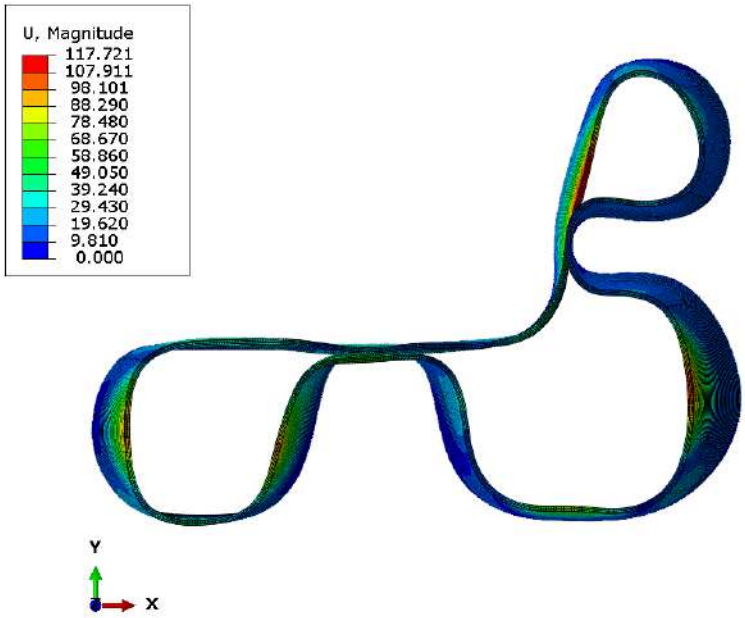

Figure 24: Deformation for case-3

Case-4: A spring constraint that is fixed in both the X and Y directions secured the part to the ground with a high stiffness of 457000000 N/mm. All degrees of freedom of the bed were constrained. In this case, the extremely high stiffness provided almost complete resistance to deformation, ensuring that the part remained essentially motionless under all applied forces. The observed distortions in the structural behavior due to this boundary condition are shown in Figure 25.

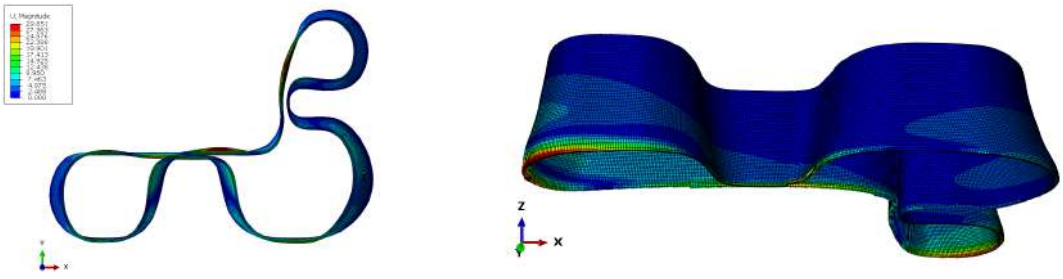

(a) (b)

Figure 25: Deformation and distortion results for Case 4: Distortion observed at the bottom of the part, with residual waviness present in the structure.

Case-5: As in previous conditions, a spring constraint fixed in both the X and Y directions secured the part to the ground with a high stiffness of 457000000 N/mm. All DOFs of the bed were constrained. The high stiffness of 4.57×10^{10} N/mm applied in this example prevented significant deformation, which made a significant difference. Upon reviewing the results of Case 4, it was evident that

the implemented boundary conditions were correct. Therefore, proceeding with material characterization, particularly focusing on thermal expansion, the value was adjusted to $8.9 \times 10^{-6}\ °C^{-1}$, achieving the desired results as shown in the Figure. 26 and distortion at the bottom of the part as shown in Figure 27.

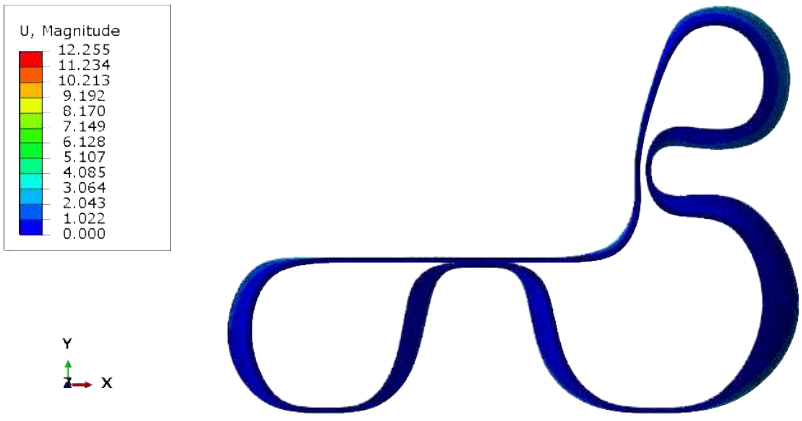

Figure 26: Deformation contour due to thermal loading, illustrating the elimination of structural waviness

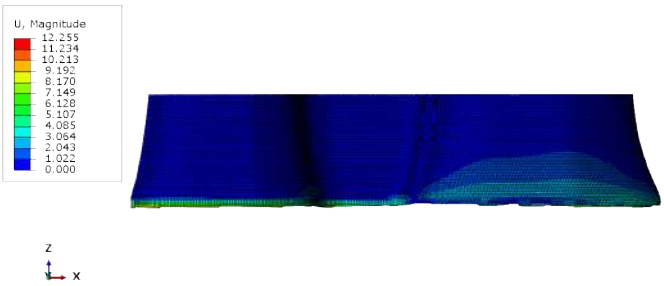

(a)

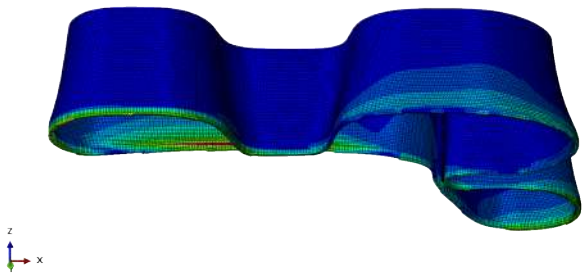

(b)

Figure 27: Illustration of the distortion observed at the bottom surface of the part

4.2.2 Residual Stress Distribution

The distribution of stresses in a printed part is important for understanding how thermally induced deformations affect its structural integrity. Internal stresses occur due to uneven cooling and the formation of thermal gradients, which can impact the strength and durability of parts made through the FDM process. It's crucial to analyze stress distribution in areas of the part where stress levels may be higher due to thermal effects see Figure 28. These stresses may lead to potential failure by cracking or warping if not properly managed. The maximum stress observed from the result is 96.4 MPa as shown in Figure 29

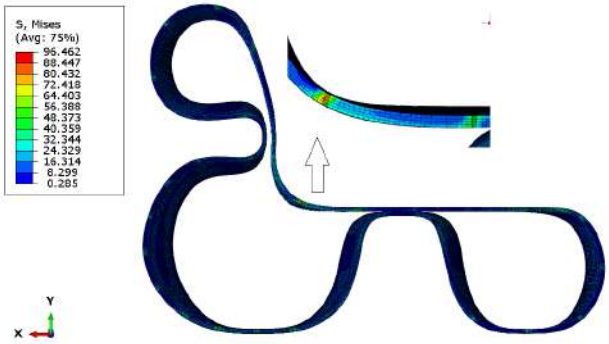

Figure 28: Residual stress distribution, indicating regions with elevated stress levels caused by thermal effects

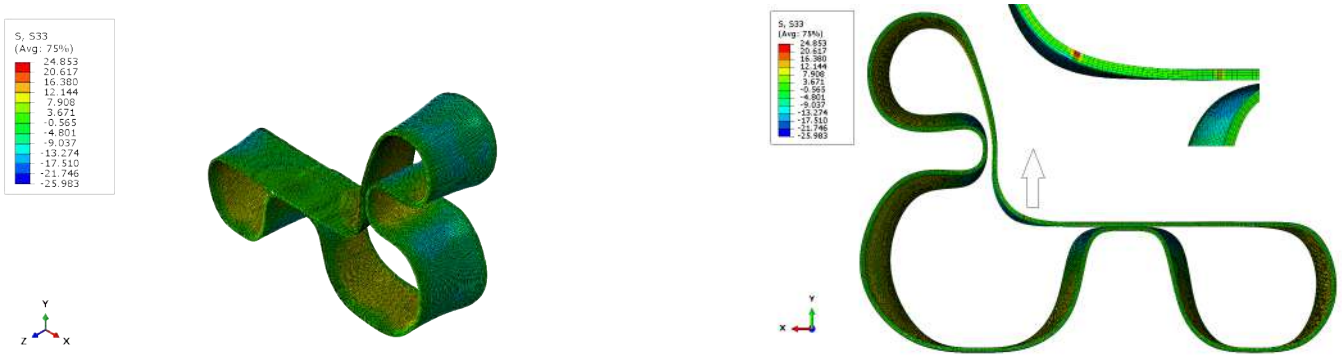

(a) (b)

Figure 29: Residual stresses observed in the Z-direction S_{33}

5 VALIDATION AND DISCUSSION

Results obtained in the previous chapter are interpreted here. This section also highlights the implications of the findings, their impacts on the FDM procedure, and recommendations drawn from the results.

5.0.1 Thermal Analysis

The comparison of the T2 experimental data with the temperature distribution from simulation results shows a strong correlation, as illustrated in Figure 15. There is a very good alignment for the T2 sensor, indicating a strong agreement between the two sets of data. This confirms that the simulation model accurately reproduces the temperature trends observed in the experimental setup. The consistency at this point demonstrates that the simulation accurately replicates real-world scenarios, further confirming the accuracy of the model.

In Figure 14, we can clearly see a difference between the experimental data and the simulated results. This is evident in the plot of the T1 experimental data with the temperature distribution obtained from the simulation results. The variation is due to the complex physics involved in the heat transfer process between adjacent printing sections. These challenges stem from the intricate physical interactions that are difficult to capture in the simulation model. The observed mismatch highlights the difficulty in accurately modeling the thermal behavior, as it is too complex to fully describe all the physical processes of heat transfer in this context.

The initial phase of the model did not include any physical complications related to heat exchange between two adjacent surfaces. To address the discrepancy between experimental and simulation data, we introduced the concept of gap conductance as discussed in section 3.6.1, depicted in Figure 6 and Figure 7. Gap conductance is a crucial parameter that characterizes heat transfer between two contacting surfaces. Its implementation has led to improved agreement between simulated and experimental temperature distributions, resulting in a better overall account of thermal interactions. This enhancement is expected to increase the accuracy of the model and provide a more realistic representation of heat transfer processes. The values for conductance are calculated using Equation 24 and can be found in Table 3.

Conductance	**Clearance**
153520	0
13800.527	0.001
1300.85	0.01
10.385	1
0.0267	5
0	10

Table 3: Gap conductance and clearance value

When gap conductance was taken into account, the simulation results started to

align more closely with the experimental data. However, there still remained a significant difference between the simulated results and the experimental data, indicating the need for further refinement. Additionally, the introduction of gap conductance caused the T2 sensor results to diverge from the experimental data, as depicted in Figure 16 and Figure 17. Even though gap conductance was not directly applied at T2, its introduction significantly altered the overall heat distribution in the part, leading to deviations at T2. This highlights the interconnected nature of thermal interactions within a system, where changes in one region can impact others due to the interdependent nature of heat transfer.

The persistent differences, despite the inclusion of gap conductance, prompted further investigation into the underlying causes. The updated results demonstrated a much closer alignment with the experimental data compared to the initial results. Nevertheless, there still existed a partial mismatch, attributed to the complex physics involved in heat transfer between two adjacent surfaces. Another potential source of this mismatch could be the inaccuracy or unavailability of data on the material properties and values used for conductance calculations, as material characterization was not performed and the data applied in the simulation model was derived from literature rather than direct measurements.

Even after incorporating the gap conductance into the model, the simulation results did not match the experimental data, as shown in Figure 16 and Figure 17. This triggered a more thorough investigation, which revealed that the film coefficient played a significant role in governing the observed variations. The film coefficient is a crucial parameter in simulating the overall thermal performance, defining the convective heat transfer between a surface and the surrounding fluid (air). It is known to be highly sensitive to the conditions at the surface and within the fluid dynamics, with its accuracy being vital for precise simulation results.

Initially, a value of 2.5×10^{-6} was assumed for the film coefficient based on general assumptions, rather than calibration. The sensitivity of this parameter prompted the implementation of an iterative optimization process. The simulation results in Figure 18 and Figure 19 showed that when $h = 2.5 \times 10^{-3}$, the results for the T1 sensor closely matched the experimental data, but the T2 sensor exhibited significant deviation.

After several iterations, a more accurate value for the film coefficient was obtained, and each correction was verified against the experimental data. This iterative refinement process confirmed that a film coefficient of $4.5 \times 10^{-3}\ ^{\circ}C^{-1}$ was closest to the experimental data, highlighting the significant impact of this parameter on the predictive accuracy of the model. This iterative refinement underscores the importance of achieving convergence in computational modeling when dealing with complex thermal interactions in the FDM.

The process of iterative refinement led to good convergence between the simulation and experimental data. A film coefficient of $4.5 \times 10^{-3}\ ^{\circ}C^{-1}$ provided the closest match to the test results. Increasing the simulation time from 5000 seconds to 7000

seconds allowed the part to reach a stabilized thermal state, as it was subjected to high temperatures during the deposition of the last few layers, compromising its integrity in the mechanical analysis. This resulted in a much smoother temperature gradient, causing slight misalignment compared to the experimental data, but still showing significant improvement. The film coefficient of 4.5×10^{-3} $^{\circ}C^{-1}$ proved to be a reliable parameter for further simulations and a good baseline for future research.

The process of identifying the film coefficient had a slight effect on the T2-sensor results, but they remained stable and close to the experimental data. This indicates that while the film coefficient variation improved other areas of the model's accuracy, the T2-sensor results were relatively unaffected and continued to fit well with the experimental data, as shown in Figure 20.

5.0.2 Mechanical Analysis

In this study, it is important to consider more realistic mechanical boundary conditions in the simulation. Typically, all six degrees of freedom are fully constrained at the bottom of a printed part, but this does not accurately represent the distortion that occurs during printing. Therefore, more realistic boundary conditions need to be applied to accurately estimate this distortion, which is crucial for predicting actual behavior. Several studies have shown that developing precise boundary conditions is essential for capturing the true distortion of parts in additive manufacturing. Traditional methods that rigidly fix the base of a part cannot provide realistic results, as flexibility and movement occur in practice.

Sequential analysis of Cases 1 to Case 4 provided valuable insight into how stiffness and boundary conditions affected the deformation behavior of the printed part.

Cases 1 to 3: In all these instances, the deformation exceeded 110 mm, preventing the expected results. The achieved deformation was unrealistically large, indicating that the applied constraints were inadequate. The low to medium stiffness allowed significant Z-direction movement, resulting in distortion not consistent with real-world behavior.

Case 4: This case, in contrast, turned out to be the breakthrough regarding the simulation. By using a very high stiffness value of 457000000 N/mm in the springs, the simulation accurately captured the part's distortion and waviness. This closely resembled the actual deformations observed during the printing process. The primary goal of the thesis was to recreate the part's waviness in the simulation, which was achieved with the inclusion of constraints. Case-4 ensures rigidity, making the simulated behavior much closer to real physical behavior observed in experimental studies.

Regarding the BC's, several scenarios were tested for effectiveness. It was found that the implementation of Case-5 was the most effective, resulting in significant improvements in simulating part distortion, making it much closer to real-world behavior. Although Case-4 didn't exactly match the physical distortions, it showed

a similar pattern, indicating its effectiveness as an approach.

While analyzing Case 4, a significant distortion at the bottom of the part was observed. The applied boundary conditions in the simulation were thoroughly checked, but the persistent wavy nature of the simulated section indicated potential errors. After investigation, it was concluded that the boundary conditions were not the source of the trouble; instead, the further distortion pointed to another factor controlling part behavior.

It was suspected that the inaccuracies might be rooted in material characterization, specifically the CTE. The initial CTE value of 8.9×10^{-5} obtained from literature did not accurately represent the material for the conditions in the study. Since precise material property data was unavailable, it was suspected that this incorrectly adopted CTE value was responsible for the differences between the simulation results and the physical behavior.

To address this, the CTE value in the simulation was changed to accurately represent the material's behavior due to thermal expansion. This led to the suspicion that the material's characterization, particularly the thermal expansion coefficient, was causing the errors. Based on this, the material's expansion value in the simulation was modified to achieve a more accurate depiction and clarify the observed changes.

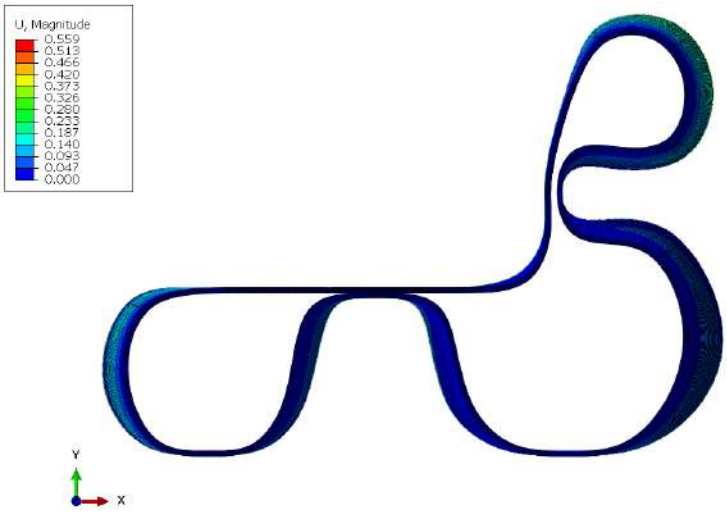

Figure 30: Results when CTE = 8.9×10^{-8} $°C^{-1}$

The impact of changing the CTE is illustrated in Figure 30. The results confirmed that the CTE significantly affects the accuracy of the simulation, as there was a notable decrease in deformation and waviness of the structure. However, reducing the initial CTE value by a factor of 1000 from 8.9×10^{-5} to 8.9×10^{-8} was neither physically accurate nor reasonable.

As seen in Figure 30, the amount of deformation decreases significantly with the change in CTE. The initial magnitude of the value assigned is not appropriate physically or meaningful. Therefore, the CTE was progressively increased to achieve

more meaningful and effective modification. Testing with a CTE of 8.9×10^{-7} $°C^{-1}$ yielded better results compared to the 8.9×10^{-8} $°C^{-1}$, as shown in Figure 31. After a few iterations, it became evident that the simulation improved significantly with a lower CTE value of 8.9×10^{-7}, providing a more accurate representation compared to values from literature and the manufactured part. This simple modification greatly decreased the predicted deformation, making determinations from this simulation statistically realistic and suggesting a high sensitivity to the CTE.

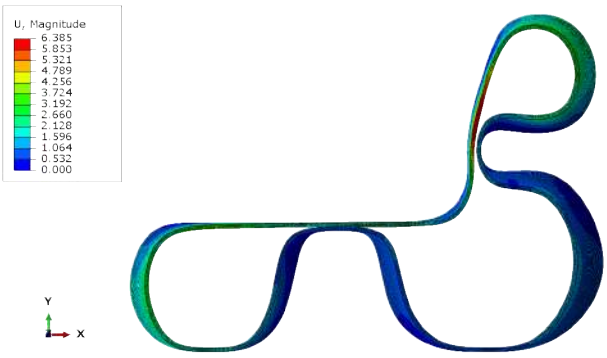

Figure 31: Results when CTE = 8.9×10^{-7} $°C^{-1}$

The optimal balance was found to produce a final CTE value of 8.9×10^{-6}. This balance minimized deformation without encountering convergence problems and large deformation, which had been issues with other CTE values. Fine-tuning the CTE was crucial for creating a simulation that closely matched real material properties and experimental observations. This careful adjustment raised the accuracy of the simulations, making the results physically meaningful and practically applicable in this study. It significantly improved the overall quality of the printed part, as illustrated in Figure 32.

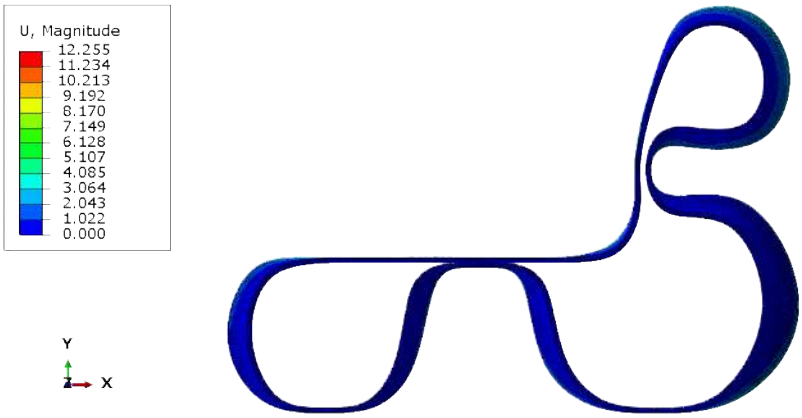

Figure 32: Result of CTE = 8.9×10^{-6} $°C^{-1}$

It's important to consider accurate material properties, especially the CTE. The discrepancies in the results are highlighted from the beginning. Improving the ac-

curacy of the CTE value significantly enhanced the simulation, ensuring practical and meaningful results.

Figure 33 (a) and (c) show warping and deformation in the real manufactured part, caused by thermal stresses and material properties. Figure 33 (b) and (d) display the predicted deformation in the simulation.

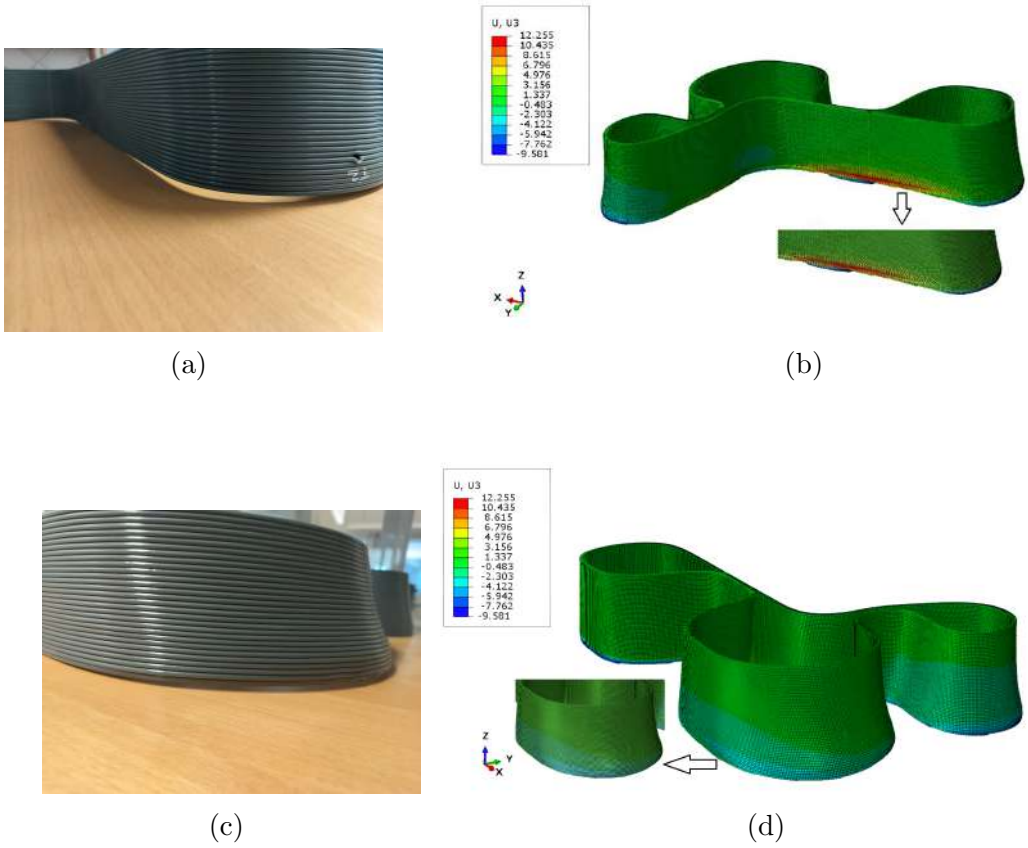

Figure 33: Comparison of real part distortion vs Simulation prediction

The simulation captures some of the main characteristics of the distortion seen in the real part, indicating that the simulation is reasonably good at reproducing the actual distortion patterns. The pattern of distortion in the simulation is similar to the real part, but there are small negative displacements where part of the model seems to penetrate the bed in Figure 33 (d), and the maximum displacement occurs at the bottom layer of the part in Figure 33 (b).

This deformation primarily occurs as a downward displacement along the Z-axis, driven by a combination of thermal contraction and the constraints imposed by the springs in the X and Y directions. Although high-stiffness springs in the X and Y directions are intended to restrict lateral movement, the significant thermal contraction of the material creates additional vertical stresses. These stresses, combined with the springs' opposition to the thermal lateral contraction, lead to the

corresponding downward deformation. This displacement is critical because it directly affects the dimensional accuracy of the part and may impair its functionality, particularly in precision-dependent applications.

The component undergoes significant deformation during the AM process, primarily due to the thermal cycles involved. The greatest deformation occurs at the bottom layer, which experiences significant temperature changes—from 225°C during deposition, to a bed preheated at 110°C, and then to a sink temperature of 42°C. Since this layer is constrained at the build platform, it undergoes substantial contraction as the material cools.

The coefficient of thermal expansion (CTE) value used in the simulation was obtained from literature for a temperature range of 55°C to 160°C, while the material was actually deposited at 225°C. This suggests that the CTE value may not accurately represent the thermal expansion behavior at elevated temperatures. Therefore, a single CTE value was used throughout the simulation for simplicity.

Based on the displacement results across different layers of the part, it is evident that the bottom layer experiences a significant amount of deformation. This is attributed to the high thermal gradient experienced by this layer during the cooling phase. As more layers are deposited, additional pressure builds on the underlying layers, particularly on the bottom layer, which is already weakened by residual stress and forcefully held down by the build platform. The cumulative interaction between thermal and mechanical loads progressively distorts the stack, with a greater propensity for deformation in the lower layers.

Understanding the relationship between thermal gradients and deposition sequence is crucial for a layer-by-layer examination of the part's general distortion. Given that the bottom layers are more readily distorted, modifying the build sequence or utilizing preheating techniques could be explored to mitigate these effects.

After the part has cooled, significant residual stresses exist in the material, greatly influencing its mechanical properties and dimensional stability. The distribution of residual stress reveals that it is most pronounced in the bottom layers, where the influence of thermal gradients is strongest during cooling. Uneven cooling rates, particularly in regions of complex geometries, such as curved regions or transitions from a flat surface to a curved one, create differential contraction and induce stress concentrations.

Additionally, the CTE value incorporated in the simulation was derived from literature for a temperature range of 55°C to 160°C, while the material was deposited at 225°C. Although a single CTE value was implemented throughout the simulation for simplicity, the potential discrepancies in thermal expansion behavior at elevated temperatures should be acknowledged. After the part has cooled, large residual stresses exist within the material, significantly influencing mechanical properties and dimensional stability. The distribution of these residual stresses is most pronounced in the bottom layers, where the influence of thermal gradients during cooling is

strongest. Uneven cooling rates, especially in regions of complex geometries such as transitions from flat surfaces to curved areas result in differential contraction and induce stress concentrations.

Residual stresses can significantly affect a part's mechanical performance. High residual stresses typically result in low fatigue resistance, leading to early failure. They can also cause warping or dimensional instability, reducing part accuracy and suitability for intended applications.

These stresses are caused by strong spring elements in the X and Y directions, which are imposed as boundary conditions in the simulation. While these springs prevent lateral movement, they contribute to vertical stresses, leading to downward deformation. This interaction emphasizes the importance of selecting appropriate boundary conditions in the simulation model, as they have a significant impact on the predicted behavior of the part.

To improve the accuracy of the simulation, further refinement is necessary. This can be achieved by adjusting the boundary conditions, material properties, and other influencing factors to predict a displacement that closely matches the real behavior of the part. Such refinement would make the simulation a more reliable tool for predicting and reducing distortion in additive manufacturing processes.

6 CONCLUSION AND FUTURE SCOPE

The research focuses on correlating the thermal and mechanical behaviors of the printed parts with experimental data for an overall sequentially coupled thermo-mechanical analysis that simulates the additive manufacturing process. The results obtained underline the complexity and challenges involved in precisely modeling these processes.

The developed simulation model was able to capture the general trends of the temperature distribution quite well and also agreed with some experimental data, such as that from sensor T2 see Figure 15). However, it differed for sensors from the T1 data as shown in Figure 14. The addition of gap conductance improved data agreement of the simulation with the experiment data to a certain extent, while some deviation persists. This emphasizes the importance of accurately modeling complex physical interactions, for instance, heat transfer between adjacent surfaces. The iterative optimization of the film coefficient also showed model sensitivity to this parameter resulting in much better matches with experimental data as shown in Figure 20 and Figure 21. For the thermal behavior, the simulation model well captured the general trends, demonstrating a good correlation with temperature distributions from the experiment.

Mechanical analysis has shown that realistic BCs are key factors governing the correct prediction of true distortion. In conventional simulations, a completely constrained bottom of a printed part across all degrees of freedom does not correspond to reality. In reality, some degree of flexibility and consequent movement cannot be avoided, and this overly rigid fixation certainly cannot capture the true distortion behavior during printing. Simulation cases through several examples showed that the development of more representative BCs was essential to capture actual distortion patterns of the printed parts. This involved the use of spring elements with high stiffness values and, especially, a well-refined coefficient of thermal expansion to greatly improve the capacity of the simulation in replicating real-world deformation characteristics, particularly at the lower layers where the thermal gradients are most pronounced during cooling. Residual stresses within these layers, as well as factors such as mechanical performance and dimensional stability, have been identified as essential in determining outcomes.

6.1 Evaluation of Research Question Outcomes

a. How does one improve FE simulation in Abaqus for the better prediction of thermal behavior and distortion in polymeric materials during their AM processes? This study also presents refinements in modeling parameters such as boundary conditions and film coefficients. These refinements will help the simulation predict thermal behavior and distortion patterns with better agreement against experimental results.

b. How do alternative boundary conditions in FE simulations affect the accuracy of distortion prediction, and what is the most appropriate setup that best

reflects real manufacturing scenarios? In order to make accurate predictions about distortion, it is necessary to have more realistic boundary conditions. The study showed that adjusting the boundary conditions and using spring elements to increase stiffness allowed the simulation to closely mimic real-world behavior. This provides valuable insights into the best boundary condition setups.

c. How does the integration of FE simulation and materials modeling in Abaqus contribute to minimizing waste in polymer AM processes while maintaining or improving product quality? The decision was made to improve the predictive accuracy of FE simulations in order to reduce the need for trial-and-error experiments and minimize material waste. This integration will lead to better resource utilization and contribute to sustainable development by improving product quality with minimal material usage.

d. How is the accuracy of FE simulations in Abaqus validated against experimental data for thermal analysis in polymer AM, and what are some of the challenges that such validation may involve? The model was validated using experimental data for thermal analysis. Although there were some challenges, such as accurately representing heat transfer, making iterative refinements to the model parameters resulted in good agreement between the simulation results and experimental observations, thus confirming the validity of the approach.

6.2 Future Scope

Further research should focus on refining the data from the T1 sensor to improve the accuracy of temperature predictions. Incorporating vertical stiffness within the Z-axis will help determine if the change results in negative displacement. This application could mitigate observed vertical distortions and provide a more representative physical behavior of printed parts. Future research should offer more details on how different process parameters impact the final product quality in additive manufacturing. This will help determine how variables such as printing speed, layer thickness, and cooling rates affect the thermo-mechanical behavior of materials, allowing for the identification of optimal conditions for AM processes. This involves fine-tuning parameters to achieve a balance between low distortion levels, high mechanical properties, and accurate dimensions in printed parts. This research could significantly enhance the reliability and efficiency of AM technologies, making them suitable for a wider range of applications.

7 APPENDIX

7.1 Derivation

Total strain is given by according to [12] [8]:

$$\boldsymbol{\epsilon} = \boldsymbol{\epsilon}^e + \boldsymbol{\epsilon}^p + \boldsymbol{\epsilon}^T \tag{27}$$

Where $\boldsymbol{\epsilon}$ is the total strain, $\boldsymbol{\epsilon}^e$ is the elastic strain, $\boldsymbol{\epsilon}^p$ is the plastic strain and $\boldsymbol{\epsilon}^T$ is the thermal strain tensors.

The elastic stress is modeled by:

$$\boldsymbol{\sigma} = \boldsymbol{D}\boldsymbol{\epsilon} \tag{28}$$

The elastic strain can be expressed as:

$$\boldsymbol{\epsilon}^e = \boldsymbol{D}^{-1}\boldsymbol{\sigma} \tag{29}$$

Where $\boldsymbol{D}$ is the material stiffness tensor, the fourth-order elasticity tensor. $\boldsymbol{\sigma}$ is the stress tensor.

For isotropic materials, the stiffness matrix in Voigt notation is given by:

$$\boldsymbol{D} = \frac{E}{(1+\nu(1-2\nu}\begin{pmatrix} 1-\nu & \nu & \nu & 0 & 0 & 0 \\ \nu & 1-\nu & \nu & 0 & 0 & 0 \\ \nu & \nu & 1-\nu & 0 & 0 & 0 \\ 0 & 0 & 0 & \frac{1-2\nu}{2} & 0 & 0 \\ 0 & 0 & 0 & 0 & \frac{1-2\nu}{2} & 0 \\ 0 & 0 & 0 & 0 & 0 & \frac{1-2\nu}{2} \end{pmatrix} \tag{30}$$

Where E is Young's modulus and ν is Poisson's ratio.

7.1.1 Plastic Strain and Deviatoric Stress

Plastic strain $\boldsymbol{\epsilon^p}$ is associated with the deviatoric part of the stress tensor $\boldsymbol{\sigma}^{dev}$:

$$d\boldsymbol{\epsilon}^p = d\lambda \frac{3}{2}\frac{\boldsymbol{\sigma}^{dev}}{\sigma_{\text{vm}}} \tag{31}$$

Where λ is the plastic multiplier or plastic flow factor.

The deviatoric stress tensor $\boldsymbol{\sigma}^{dev}$ is given by:

$$\boldsymbol{\sigma}^{dev} = \boldsymbol{\sigma} - \frac{1}{3}\text{tr}(\boldsymbol{\sigma}) \cdot \mathbf{I} \tag{32}$$

where tr($\boldsymbol{\sigma}$) is the trace of the stress tensor ($\boldsymbol{\sigma}$), which is the sum of the diagonal stresses, $\mathbf{I}$ is the identity tensor.

7.1.2 Thermal Strain

As temperature fluctuates in the material the thermal strain $\boldsymbol{\epsilon}^T$ is given by:

$$\boldsymbol{\epsilon}^T = \alpha(T) \cdot (T - T_0) \cdot \mathbf{I}_v \tag{33}$$

Where $\alpha(T)$ is the coefficient of thermal expansion, which is temperature-dependent, T is the current temperature, and T_0 is the reference temperature. $\mathbf{I}_v$ is the vector form of the identity tensor in Voigt notation $\{1, 1, 1, 0, 0, 0\}^T$.

7.1.3 Von Mises Stress and Yield Criterion

Plastic strain is often calculated by von-Mises stress σ_{vm},

$$\sigma_{vm} = \sqrt{\frac{3}{2}\boldsymbol{\sigma}^{dev} : \boldsymbol{\sigma}^{dev}} \tag{34}$$

The plastic multiplier λ is defined based on the yield criterion:

$$d\lambda = \begin{cases} 0, & \text{if } \sigma_{vm} < \sigma_p \\ > 0, & \text{if } \sigma_{vm} \geq \sigma_p \end{cases} \tag{35}$$

Where σ_p is the yield stress of the material.

7.1.4 Stress-Strain Relationship Considering Thermal Effects

An effective measure of stress used in yield criteria is defined by:

$$\boldsymbol{\sigma} = \mathbf{D}(T) \cdot \left(\boldsymbol{\epsilon} - \boldsymbol{\epsilon}^T - \boldsymbol{\epsilon}^p\right) \tag{36}$$

Expanding this with the definitions of the strain components, we get:

$$\boldsymbol{\sigma} = \mathbf{D}(T) \cdot \left(\boldsymbol{\epsilon} - \alpha(T)(T - T_0) \cdot \mathbf{I}_v - d\lambda \frac{3}{2} \frac{\boldsymbol{\sigma}^{dev}}{\sigma_{\text{vm}}}\right) \tag{37}$$

7.2 GAP conductance

To calculate the gap conductance, several literature sources were consulted to identify the appropriate equation. One notable resource was the thesis by Afazov[15]. A contact between two interfaces, denoted by nodes 1 and 2, that have respective

clearances of d and temperatures T1 and T2. When $d > 0$, there is a space between two solid contacts. Usually, air or another gas is used to fill the gap.

$$q_g = q_c + q_r \tag{38}$$

where q_c is the gas conductance heat transfer and q_r is the radiation heat transfer.

The gas conductance heat transfer q_c can be calculated by:

$$q_c = \frac{k_g(T_1 - T_2)}{d} \tag{39}$$

where, k_g is the thermal conductivity of the gas, T_1 and T_2 are the temperatures at the respective nodes, d is the gap clearance.

$$q_c = \frac{k_g(T_1 - T_2)}{d + d_r + g_1 + g_2} \tag{40}$$

Where g1 and g2 are the temperature jump distances for nodes 1 and 2 of the contacting pair, which are provided by and dr is associated with the roughness of the two contacting surfaces.

The temperature jump distances g_1 and g_2 are given by:

$$g_1 = \frac{k(2 - a_1)\sqrt{2\pi T_1}}{P a_1 R(\gamma + 1)} \tag{41}$$

$$g_2 = \frac{k(2 - a_2)\sqrt{2\pi T_2}}{P a_2 R(\gamma + 1)} \tag{42}$$

Where γ is the specific heat ratio for the corresponding interface material, and is the accommodation coefficient for the corresponding interface material, R is the universal gas constant, and Pg is the gas pressure.

The radiation heat transfer q_r between the two surfaces is given by:

$$q_r = f\sigma_{SB}(T_1^4 - T_2^4) \tag{43}$$

Where T1 and T2 are the temperatures in nodes 1 and 2, f is the radiation factor, and σ_{SB} is the Stefan-Boltzmann constant.

The heat transfer can be defined as:

$$q = h(T_1 - T_2) \tag{44}$$

Where h is the coefficient of gap conductance, q is the heat transfer, and T1 and T2 are the temperatures of two surfaces.

The heat transfer equilibrium equation is:

$$q = q_g = q_c + q_r \tag{45}$$

or

$$h(T_1 - T_2) = \frac{k_g(T_1 - T_2)}{d + d_r + g_1 + g_2} + \frac{\sigma(T_1^4 - T_2^4)}{\frac{1}{\epsilon_1} + \frac{1}{\epsilon_2} - 1} \tag{46}$$

Another reference taken was from the work of [16]

The conductance across the surfaces is given by radiant heat transfer term, h_r, solid conductance across contact areas when the gap is closed, h_s, and heat transfer over the gap via conduction through the gas, h_g.

$$h = h_g + h_s + h_r \tag{47}$$

$$h_g = \frac{k}{d + d_{min} + g_f + gc} \tag{48}$$

where g_f and g_c are the "temperature jump distances" at the fuel and cladding surfaces, respectively, and d_{min} is a measure of the roughness of the two surfaces.

References

[1] "The research institute of sweden — rise." (), [Online]. Available: https://www.ri.se/en/about-rise.

[2] Produktion, *Organizing the circular economy through a network of LSAM Microfactories Recycling Ocean Plastics (OCEAN-LSAM) - Produktion2030*, Oct. 2022. [Online]. Available: https://produktion2030.se/en/projekt/organizing-the-circular-economy-through-a-network-of-lsam-microfactories-recycling-ocean-plastics-ocean-lsam/.

[3] R. Kumaresan, M. Samykano, K. Kadirgama, W. Harun, and P. D. M. M. Rahman, "Fused deposition modeling: Process, materials, parameters, properties, and applications," *The International Journal of Advanced Manufacturing Technology*, vol. 120, May 2022. DOI: 10.1007/s00170-022-08860-7.

[4] A. Cattenone, S. Morganti, G. Alaimo, and F. Auricchio, "Finite element analysis of additive manufacturing based on fused deposition modeling: Distortions prediction and comparison with experimental data," *Journal of Manufacturing Science and Engineering*, 2018. [Online]. Available: https://api.semanticscholar.org/CorpusID:116378914.

[5] M. Srivastava and S. Rathee, "Additive manufacturing: Recent trends, applications and future outlooks," *Progress in Additive Manufacturing*, vol. 7, no. 2, pp. 261–287, 2022.

[6] *Thermomechanical Analysis of Powder Bed&x2013;Type Additive Manufacturing Processes Using the Trajectory-Based Method — docs.software.vt.edu*, https://docs.software.vt.edu/abaqusv2023/English/SIMACAEANLRefMap/simaanl-c-amspecialpurpose-powderbed.htm#simaanl-c-amspecialpurpose-powderbed-activation, [Accessed 09-09-2024].

[7] P. Michaleris, "Modeling metal deposition in heat transfer analyses of additive manufacturing processes," *Finite Elements in Analysis and Design*, vol. 86, pp. 51–60, 2014.

[8] M. Gouge and P. Michaleris, *Thermo-mechanical modeling of additive manufacturing*. Butterworth-Heinemann, 2017.

[9] , *Use abaqus to simulate additive manufacturing printing a hip implant*, 2020. [Online]. Available: https://simulation-blog.technia.com/simulation/using-abaqus-to-simulate-additive-manufacturing-printing-an-optimized-hip-implant.

[10] *MatWeb - The Online Materials Information Resource*. [Online]. Available: https://www.matweb.com/errorUser.aspx?msgid=2&ckck=nocheck (visited on 09/29/2024).

[11] K. Khanafer, A. Al-Masri, I. Deiab, and K. Vafai, "Thermal analysis of fused deposition modeling process based finite element method: Simulation and parametric study," *Numerical Heat Transfer, Part A: Applications*, vol. 81, no. 3-6, pp. 94–118, 2022.

[12] N. Ahmed, I. Barsoum, and R. K. A. Al-Rub, "Numerical investigation of residual stresses in thin-walled additively manufactured structures from selective laser melting," *Heliyon*, vol. 9, no. 9, 2023.

[13] M. J. Abarca, "Development of a low fidelity process model for additive manufacturing," M.S. thesis, Universidade do Porto (Portugal), 2020.

[14] *ABAQUS Analysis User's Manual (v6.6)*. [Online]. Available: `https://classes.engineering.wustl.edu/2009/spring/mase5513/abaqus/docs/v6.6/books/usb/default.htm?startat=pt09ch30s02aus147.html` (visited on 09/27/2024).

[15] S. Afazov, "Modelling of thermal gap condutance in casting using finite element analysis," *Manuf. Technol. Center*, pp. 1–11, 2013.

[16] H. C. Kim, Y. S. Yang, D. H. Kim, J. G. Bang, S. K. Kim, and Y. H. Koo, "Study of gap conductance model for thermo-mechanical fully coupled finite element model," in *Transactions of the Korean Nuclear Society Autumn Meeting, Gyeongju, Korea*, 2012.